ELSEVIER

Solar Energy Materials & Solar Cells 76 (2003) 431–487

Solar Energy Materials & Solar Cells

www.elsevier.com/locate/solmat

Low temperature polycrystalline silicon: a review on deposition, physical properties and solar cell applications

J.K. Rath*

Debye Institute, Surface, Interface and Devices, Utrecht University, Princetonplein 4, P.O. Box 80000, 3508 TA Utrecht, Netherlands

Abstract

This review article gives a comprehensive compilation of recent developments in low temperature deposited poly Si films, also known as microcrystalline silicon. Important aspects such as the effect of ions and the frequency of the plasma ignition are discussed in relation to a high deposition rate and the desired crystallinity and structure. The development of various ion energy suppression techniques for plasma enhanced chemical vapour deposition and ion-less depositions such as HWCVD and expanding thermal plasma, and their effect on the material and solar cell efficiencies are described. The recent understanding of several important physical properties, such as the type of electronic defects, structural effects on enhanced optical absorption, electronic transport and impurity incorporation are discussed. For optimum solar cell efficiency, structural considerations and predictions using computer modelling are analysed. A correlation between efficiency and the two most important process parameters, i.e., growth rate and process temperature is carried out. Finally, the application of these poly Si cells in multijunction cell structures and the best efficiencies worldwide by various deposition techniques are discussed.

Keywords: Polycrystalline; Silicon; Thin film; Solar cell; Chemical vapour deposition

1. Introduction

Among the many competing technologies for photovoltaic devices, the crystalline silicon (c-Si)-based solar cell has been the most successful, in industrial production as

*Tel.: +31-30-253-2961; fax: +31-30-254-3165.
E-mail address: j.k.rath@phys.uu.nl (J.K. Rath).

0927-0248/02/$ - see front matter © 2002 Elsevier Science B.V. All rights reserved.
PII: S0927-0248(02)00258-1

well as in shipments. It must be remembered that the c-Si-based photovoltaic industry has mostly benefited from the rejects of the production of integrated circuits (IC). Even while considering other sources, the scarcity of feed stock will be a bottleneck for sustaining a growth rate of 20–25% up to 2020, as envisioned by the road map for the US industry [1]. Thin film deposition on large area substrates, high throughput and the effective use of source gas is an attractive alternative. As a technology, amorphous silicon (a-Si:H)-based device fabrication has already proved to be mature enough to meet all demands. However, the limitation to the efficiency and the additional light-induced degradation effect put a question mark on the achievable goal. Thin film silicon can step in as a technology which can utilise the best of c-Si (efficiency) and amorphous silicon (fast industrial production) technology. A futuristic prediction [2] of different technologies shows that both c-Si and amorphous silicon technologies have almost reached the maximum efficiencies achievable, whereas thin film silicon still has a lot of room for development and can reach a high efficiency ($\sim 30\%$). At this juncture, it is necessary to define poly Si. Thin film silicon should be differentiated from high temperature ($>1400^{\circ}C$) bulk poly Si. This category of material includes two approaches; high temperature ($>600^{\circ}C$) and low temperature ($<600^{\circ}C$) growth. The criterion for differentiation is set by the types of substrate that can be used (for example for glass substrates, a low growth temperature is required). However, there is one more criterion, i.e., the hydrogen effusion maximum at $\sim 600^{\circ}C$, due to which low temperature processes can yield material with passivated grain boundaries during growth, whereas high temperature films invariably need a second step for hydrogen passivation. This low temperature polycrystalline silicon (poly Si) is also called microcrystalline silicon (μc-Si). To avoid confusion, we can define poly Si as a material with large grains ($\geqslant 100$ nm—no amorphous phase, only crystalline grains and grain boundaries), whereas μc-Si is defined as a material (containing amorphous tissues, crystalline grains and grain boundaries) with small grains, typically ~ 20–30 nm. In this review article, we will mostly concentrate on this low temperature approach.

A complete microcrystalline silicon cell made by very high-frequency plasma enhanced chemical vapour deposition (VHF PECVD) with an efficiency of 4.6% [3] opened up a new area of photovoltaic development. However, cell efficiencies were limited by low open circuit voltages and fill factors. The main attention of these cells is the stability to light soaking and a long wavelength response. However, improvement in the efficiency of the single junction and application as a bottom cell in a tandem concept (''Micromorph''), which showed an initial efficiency of 13% [4], looked like a breakthrough in the low temperature process. A quick adaptation of this concept, and its translation into industrial production by Kaneka Corporation has established the technological viability of this low temperature process. This rapid adaptation was possible due to the maturity of the amorphous silicon technology, including the back reflector, the transmitting conducting oxide (TCO), monolithic integration and encapsulation. The use of μc-Si cells as red-light absorbing structures in multijunction cells with a-Si top cells absorbing the blue-green light would lead to elimination of costly germanium gas from the fabrication process.

2. Deposition techniques

Chemical vapour deposition (CVD) is the most widely used process for making poly Si films. In such a process a source of gas, for example SiH_4, is decomposed in several possible ways such as plasma (PECVD), catalysis (Hot-wire CVD), etc. In most cases, the source gas is diluted with hydrogen to obtain the poly Si growth regime, whereas amorphous silicon is generally obtained with pure silane (SiH_4). The decomposed species after a series of gas phase reactions reach the substrate and deposit. One can also use a two step process where amorphous silicon deposited by CVD is subsequently crystallised through solid phase crystallisation (SPC), laser annealing, chemical annealing, etc.

2.1. Plasma enhanced chemical vapour deposition (PECVD)

This deposition process is based on electron impact dissociation of a process gas such as silane in a plasma. A low-pressure weakly ionised plasma created between two electrodes contains positive, negative and neutral species (radicals). The powered electrode is called the cathode and the grounded anode electrode is where the substrate is attached for deposition. As the substrate and electrodes are slightly negative with respect to the plasma bulk, negative ions are trapped in the plasma. Under high-pressure conditions, this creates dust by reacting with the silane. The positive ions and the radicals reach the substrate by drift and diffusion, respectively, and undergo surface and subsurface reactions during deposition. For poly Si deposition, the atomic hydrogen flux reaching the growing surface plays an important role in crystal nucleation.

2.1.1. Role of ions

Radicals are considered to be the main precursors for the growth of both amorphous and microcrystalline silicon in a PECVD deposition process. It is agreed from many reports that SiH_3 is the main precursor for the device quality films. Low lifetime radicals, higher silane radicals (Si_2H_5, Si_3H_8, etc.) and reactive radicals (SiH_2, SiH, etc.) are considered a hindrance to microcrystalline deposition. However, it is mainly the ions which determine the final film quality. The ion flux density reaching the substrate is determined by the ion density in the plasma (electron density), whereas the kinetic energy of individual ions reaching the substrate is determined by the electron temperature in the plasma. Whereas ions with energy $> 5\,eV$ are shown to be beneficial to amorphous silicon formation [5], high-energy ions seem to have adverse effect on crystallinity. In fact, it has been shown that with the same type of plasma it is only the presence or non-presence of ions (at the growing film), which determines whether it is amorphous or microcrystalline. However, it has to be emphasised that the presence of ions is not as bad an effect as their energy [6]. In fact, a high ion flux in the high-frequency case would give rise to enhanced surface diffusion of impinging species, even at a low substrate temperature (T_s), which is a necessary condition for good crystallinity.

One of the methods for varying the ion bombardment is to choose the frequency of the power source generating the plasma. An earlier report [6] in the case of VHF PECVD explained high crystallinity in the VHF process compared to 13.56 MHz samples as due to the presence of high-energy ions in the latter case. This model is based on the criterion that the energy of the impinging particles on the growth surface must not exceed the threshold energy of defect formation. The plasma contains both silicon and hydrogen ions, but the effect of the latter is considered negligible. The peak of the ion energy distribution is a function of excitation frequency. As a result, the peak ion energies for excitation at 70 MHz or higher frequencies are around 14 eV, which is lower than the threshold energy of 16 eV for Si impact. In contrast to this, for the case of 13.56 MHz excitation, the peak of the ion energy value is around 45 eV. Another way of controlling ions which has been proposed is to use deuterium instead of hydrogen dilution. In PECVD, this has shown to improve the crystallinity and decrease the defect density. The reason suggested is that deuterium dilution leads to lower ion bombardment, due to a lower electron temperature in the plasma formed. This is attributed to the heavier mass of deuterium, which results in a lower electron loss rate [7].

The second method to manipulate the ion bombardment at the growing surface is through the design of the electrode configuration. An attempt to grow microcrystalline films by suppressing ions from reaching the substrate surface has shown promising results, as proposed by Veprek et al. [8]. A triode technique, in which there is a negatively biased mesh electrode between the plasma and the substrate (as proposed by Matsuda [9]), is very effective. Shirai et al. [10], using a high-density microwave plasma, showed that films with (2 2 0) grain orientation could be made by using a mesh grid electrode in a deposition from an Ar diluted SiH_4 system. They demonstrated that the elimination of the Ar ion energy in combination with H_2 dilution and a higher T_s promoted a preferential (2 2 0) orientation. Nishimiya et al. [11] used a novel PECVD technique employing a biased wall (BW) method in which there is a positively DC BW electrode, surrounding the plasma between the cathode and the anode. The lateral component of the electric field forces positive ions to escape laterally from the plasma, causing a reduction in ion bombardment. The advantage of the BW method is that ion bombardment can be reduced without reduction of the deposition rate. With this deposition technique operating at 13.56 MHz, microcrystalline silicon films (grain size of 20 nm) have been produced at a high growth rate of 0.6 nm/s, at $T_s = 350^{\circ}C$.

Kondo and Matsuda [7] tried to resolve the controversy regarding the role of ionic species in crystalline growth; i.e. whether ion bombardment is beneficial [12] or disruptive [13,14] to growth. It is found that suppression of the ion energy is more effective for improving crystallinity, especially at high growth rates [7]. Another effect of ion bombardment is the randomisation of preferential orientations of grains with an increase in ion bombardment [7], whereas preferential (2 2 0) orientation is considered beneficial for solar cell applications (see Section 5.1.3).

The effect of ion bombardment on the deposition is best observed in the case of the electron cyclotron resonance (ECR) CVD process. Here, due to remote deposition, the ion energy and flux at the substrate can be independently modified

without affecting the plasma. De Boer et al. [15], using the ECR process, observed that even when growing crystalline Si epitaxial layers on Si wafers, high ion bombardment (increasing bias voltage) led to an increase in the Raman line width and a decrease in the electron mobility in the film. Nozawa et al. [16], from Nagoya University, observed in the case of ECR CVD that increasing the positive DC bias to the substrate improved the crystallinity. This was attributed to a decrease in the ion flux to the substrate (also a change in the dominant ion flux, which changes from SiH_3^+ to SiH^+ and Si^+ with bias voltage varying from 0 to +50 V). One interesting observation is that application of a positive bias to the substrate does not have much effect on the deposition rate (0.2 nm/s). However, the structure is greatly affected (preferential (2 2 0) orientation, promotion of longitudinal growth, no cracks in the film). For a negative substrate bias, the ion energy is sufficient to destroy the crystalline structure. With optimisation of the substrate bias, films grown at 300°C showed a grain size of 200 nm [16]. A similar effect of DC bias was observed by Birkholz et al. [17] while making poly Si films on stainless steel (SS) substrates by ECR CVD from a SiH_4/H_2 gas mixture. Excluding the charged species from the substrate [18] by using a permanent magnet in an ECR deposition system resulted in microcrystalline films with a 55% crystalline volume fraction, grown at a substrate temperature of 150°C. It is speculated that hydrogen ions etch the a-Si:H, whereas atomic hydrogen promotes the Si-network, as a result of which a smoother surface (RMS roughness 3.0 nm, grain size 50 nm) is formed when charged species are suppressed. However, as we will see in the case of HWCVD, even deposition without hydrogen ions does lead to a high surface roughness. A reversal of the orientation from (2 2 0) to (1 1 1) is observed with a change of bias from 0 to +15 V [17]. At a critical bias level of 15 V, poly Si films of high density and low oxygen content, small microvoid density and large (42 nm) grains have been obtained. A reduction of the deposition rate with positive bias has been explained by assuming that ions generally contribute a large part (70% in case of PECVD) to the deposition of μc-Si. It is claimed that the case of deposition with a positive substrate bias is similar to the HWCVD case, where only radicals contribute to the growth and both cases have a similar surface roughness.

On the other hand, in ECR-CVD, the presence of an RF (13.56 MHz) substrate bias [19] decreases the crystallinity. Films deposited without a bias develop a very uniform columnar structure, whereas films grown with a bias develop a closely packed continuous but more amorphous structure. This is attributed to the increase in ion to radical ratio and the reduced effect of hydrogen radicals on the growing films. This can be understood from the fact that an RF gives a negative self-bias to the substrate, because fast electrons can build up negative charges on insulating substrates. This accelerates and attracts more ions to the growing surface, which not only dominates over the role of neutral radicals, but also the impact of an accelerated ion flux in disordering the growing surface is expected.

The effect of ions on microcrystallinity is not confined to PECVD cases, but is more universal. Its effect is also observed in other techniques for the deposition of μc-Si. Sputtering is one suitable technique for preparing amorphous and microcrystalline silicon at high deposition rates. The presence of ions and high

energetic neutrals is one of the main limitations, as high-energy ions are believed to affect adversely the nucleation process and the defect density. One solution is to use an ICP-based ionised magnetron sputtering [20], where fast sputtered neutrals are effectively thermalised and ionised by a high gas pressure and the kinetics of the ionised species are controlled by an appropriate substrate bias. The main advantage of this technique is thought to be ionisation of the depositing silicon flux and retardation of ionised fast-reflecting neutrals such as hydrogen atoms. Microcrystalline films, grown at temperatures of 250°C and lower, can be produced at a deposition rate of 13.3 nm/s, with grain sizes of 70–80 nm.

A beneficial effect of ions has also been reported. Some of the cases are presented here. Shin et al. [21] deposited poly Si by plasma immersion ion implantation using an ECR plasma of pure SiH_4. Implantation was achieved by immersing the target into the plasma and biasing it negatively between -5 and -15 V. Both Si and hydrogen ions are implanted into the sample. However, the rate at which Si atoms are displaced by the implanted hydrogen is 1% of the rate at which they are displaced by implanted Si ions. Compared to films deposited without implantation, ion implanted films have larger grains (10–100 nm, average 21 nm) and a lower grain density. A dense film without incubation (no need for a seed layer) has been obtained at a low substrate temperature of 410°C. Two possible effects of the ion beam have been speculated: (i) a surface effect: very small grains do not survive the high dose of ion irradiation ($1 \times 10^{17}\,cm^{-2}\,s^{-1}$) during an ion pulse, thereby reducing the nucleation rate, (ii) a bulk effect: the ion beam induces grain growth. Non-equilibrium defect densities and atomic mobilities are identified as the dominant factors in determining the effect of ions.

Poly Si films grown at temperatures below 650°C can be made at a deposition rate of 13 nm/s at (550°C) by ion assisted physical vapour deposition, which uses a small fraction of ionised silicon atoms within the Si beam. The accelerated Si^+ ions provide hyperthermal energy for the epitaxial growth [22].

One variation of the remote plasma technique is called electron beam excited chemical vapour deposition (EBEP-CVD) [23]. In this, an electron beam from a LaB_6 filament source during a DC arc discharge between the filament and electrode is directed to a reaction chamber where collision of electrons (with energies tuned to 100 eV) with silane molecules (without hydrogen dilution) creates the plasma. This behaviour is in contrast to PECVD, where there is a spectrum of electron energies and only a small fraction of electrons have a high enough energy to ionise hydrogen. High-energy electrons (100 eV) not only crack the SiH_4 molecule ($\sim$4 eV) but can also ionise atomic hydrogen ($\sim$14 eV). The presence of atomic hydrogen or hydrogen ions in the vicinity of the growing surface causes the successful growth of microcrystalline silicon over a wide range of growth conditions. This experiment shows a novel way of increasing the window of parameters for microcrystalline deposition, although the deposition rate achieved is only 0.1 nm/s. Microcrystalline films with a hydrogen content of 19% are made, which may have interesting consequences for the passivation of grain boundaries.

The above observations indicate that in most cases (*especially low temperature processes*) a high ion impact has an adverse effect on the crystallinity. This effect

restricts the use of increasing power in a PECVD process to achieve deposition at high growth rates. At this point, it should be emphasised that there are two distinct features involved here, the ion density and the ion energy. There is no evidence that the former retards nucleation, rather, it may help, whereas the latter has a negative effect. One of the paths followed is to use high frequency. In the next section and that covering solar cells, we will follow the effect of frequency on physical properties such as the deposition rate and the solar cell efficiency. Another way to solve the problem is to completely eliminate the ions. From this point of view the photo-CVD, expanding thermal plasma (ETP) and HWCVD deposition processes have a distinct advantage. However, as we will see in the solar cell results, the best efficiencies are still achieved by Plasma CVD. There is a proposition that there are two types of growth regime for the transition from amorphous to microcrystalline silicon [24]:

(1) The main precursor is SiH_3 and crystallinity is caused by enough atomic hydrogen. The example is PECVD deposition where the surface reaction probability of the depositing species is ~ 0.2.
(2) Abstraction reactions in the gas phase, leading to Si and sufficient hydrogen to result in microcrystallisation. Examples are ETP and HWCVD where the surface reaction probability is around 0.56 [24].

2.1.2. Materials obtained at various frequencies

Ion bombardment is either beneficial or has an adverse effect, depending on the deposition conditions. It is reported that ions can contribute up to 70% of the growth in PECVD deposition of μc-Si [25]. Suppression of the ion energy is effective in improving the crystallinity, particularly at high growth rates. The ion energy depends on gas pressure, exciting frequency and the electrode configuration. The ion density in the plasma is determined by the electron density, whereas the kinetic energy of the ions is determined by the electron temperature. High excitation frequencies result in a greater electron density and a lower electron temperature [26]. The average electron energy decreases with increasing frequency [27]. In a diode type reactor, the frequency of the plasma excitation source has a direct correlation with the ion energy. The peak-to-peak voltage (V_{pp}) at the electrodes is strongly reduced at high frequencies. A lower V_{pp} is indicative of a lower ion peak energy. The maximum ion energy at the substrate surface is given by $(eV_{pp})/4$, where e is the electronic charge. A systematic reduction of the maximum ion energy at the substrate with increasing frequencies has been observed [28]. This results in lower energy bombardment at the growing surface at higher frequencies. In this section, we will evaluate the best physical properties of microcrystalline materials obtained at various frequencies. In all cases it is observed that the optimisation procedure has been carried out keeping in mind the target of a high deposition rate.

RF 13.56 MHz: Guo et al. [29] first obtained μc-Si films at a high growth rate of 0.93 nm/s, by employing a combination of a high deposition pressure of 4 Torr and silane depletion in a conventional RF PECVD deposition system, in a regime called

high-pressure depletion (HPD). The ion energy can be effectively controlled by the gas pressure. In addition to the advantage of a high radical generation rate (high growth rate) and a lower plasma potential (lower ion energy) this has the disadvantage of a low atomic hydrogen density due to the annihilation reaction $H + SiH_4 \rightarrow SiH_3 + H_2$. This disadvantage is compensated by deposition in a depletion regime, which can be achieved using a high RF power. This leads to a deposition method called HPD, as proposed by the ETL group in Japan [29]. Using this method, μc-Si films deposited at a rate of 1.5 nm/s have been obtained [7].

Yamamoto et al. [30] made poly Si films at a deposition rate of 1.5 nm/s by RF PECVD, at a substrate temperature of $\sim 550^{\circ}C$.

Some of the other RF deposition processes are:

(1) RF cathode type PECVD [31] and
(2) cyclic CVD [32].

A variation of the PECVD process is inductively coupled plasma CVD (ICP-CVD) [33]. Such a process has the advantage of a high plasma density of $\sim 10^{12}\,cm^{-3}$, less ion bombardment on the growing surface and good uniformity. At a substrate temperature of 300°C, (1 1 1) preferentially oriented microcrystalline silicon films (grain size 120 nm) have been made from a gas mixture of $SiH_4/SiCl_2/H_2$ in a 13.56 MHz RF plasma, at a growth rate of 0.42 nm/s. N–i–p Cells (glass/MoW/polycrystalline n–i–p) with an efficiency of 3.14% ($V_{oc} = 0.23$ V, $J_{sc} = 19.7\,mA/cm^2$, FF = 0.54 at $79\,mW/cm^2$) have been obtained.

VHF: The VHF CVD technique is the first successful one to obtain device quality μc-Si for solar cells [3], and a number of groups have followed this deposition process for μc-Si. In such a method, a frequency range of 20–110 MHz is generally used, though the best μc-Si is obtained around 50–110 MHz. Research at IMT Neuchatel [4] showed that device quality microcrystalline films with a low defect density ($\sim 10^{16}/cm^3$) could be made by VHF. A higher deposition rate (~ 0.1 nm/s) compared to standard 13.56 MHz deposited μc-Si films is also a technological advantage. Since then, an increase in the deposition rate has been the main thrust. A frequency increase combined with the HPD could further enhance the deposition rate, which for example is 3.8 nm/s at 60 MHz at $T_s = 250^{\circ}C$ [7].

Use of two configuration related changes, i.e., a triode configuration and a showerhead for the gas flow, have further improved the deposition rate. Suzuki et al. [34] combined the VHF PECVD and HPD method with these modifications, and were able to deposit films at a rate of 5.8 nm/s. A variety of electrically grounded mesh cathodes with transmittances of 49%, 64%, and 81% were tried. The use of a mesh changed the film growth from purely amorphous to microcrystalline with only a 9% reduction in the thickness, which is amazing considering the shadowing effect of the mesh. It was considered that a hollow-cathode-like discharge on the mesh holes promoted the decomposition of SiH_4 and realised the high rate growth of μc-Si. The role of the shower cathode is to improve the uniformity, in addition to improving the quality of the films. An important observation is that the growth rates

are three times faster with a showerhead than with a normal gas flow. This is attributed to an increased SiH_4 density in the cathode–anode space. The properties of films deposited by the above method are a 33 nm grain size (XRD (220) preferential), $\sigma_{ph}/\sigma_d = 10^2$ and $N_d = 2.5 \times 10^{16}\,cm^{-3}$.

An adaptation of the VHF process is the static closed chamber process [35] (SCC VHF-GD), which delivers a deposition rate of 0.6 nm/s with a low silane consumption of 1 sccm and without the need for hydrogen feed stock gas, though cell efficiencies are too small ($\eta = 1.2\%$). The defect density is a factor of two higher than in standard VHF films.

UHF: Takashima et al. [36] deposited microcrystalline films in a plasma system at an ultra high frequency (UHF) of 500 MHz from a gas mixture of SiH_4 and H_2. In a UHF plasma, the low electron temperature and high electron density enable the achievement of high crystallinity. An atomic hydrogen density of $8 \times 10^{11}\,cm^{-3}$ is estimated in the chamber at a silane to hydrogen ratio of 1–2.5%; the regime where the high crystallinity has been obtained. A crystalline fraction of 93%, with an ultra thin incubation amorphous layer of 3 nm has been achieved [36].

ECR-CVD: This is a remote plasma deposition process, in which highly reactive H radicals generated by microwave excitation (2.45 GHz) in an electron cyclotron resonance plasma generator flow towards the substrate (which is located several centimeters downstream of the resonant point of the plasma). Here, they combine with silane and produce silyl (SiH_3) radicals which then lead to film growth. By this process, Moradi et al. [37] made poly Si at 400°C, at a deposition rate of 0.13 nm/s. Films with randomly oriented grains with grain sizes of 20–30 nm had an electron mobility (Hall) of $12\,cm^2/V\,s$. However, the high dark conductivity of $1.6 \times 10^{-4}\,\Omega^{-1}\,cm^{-1}$ and activation energy of 0.18 eV showed an n-type character, which is generally attributed to oxygen contamination.

Bae et al. [19] could deposit poly Si by ECR-CVD at a substrate temperature of 120°C and a low dilution of $SiH_4/H_2 = 1/3$. The fact that so little hydrogen dilution is needed compared to standard PECVD was attributed to the high density of the plasma, which leads to a high concentration of atomic hydrogen. The films, with randomly oriented grains, had a conductivity activation energy of 0.62 eV, which showed their intrinsic character. Poly Si films with a crystalline fraction of 70% at a substrate temperature of 300°C can be made by ECR CVD from 2% SiH_4/Ar further diluted in H_2 [38], at a hydrogen dilution level of $H_2/SiH_4 = 0.55$. However, crystallinity can also be achieved without hydrogen dilution, although the crystalline fraction is lower, at 45%.

Though the ECR technique has many advantages, so far no reports of a very high growth rate or good solar cell efficiencies has been made.

Microwave: The difference between microwave PECVD and ECR CVD is that the plasma in the former case is not in a resonance condition. The dissociation of a source gas (such as SiH_4) is either remote (as in ECR CVD) or direct in the plasma. In such a process, the increased ion flux achieved while keeping the ion bombardment energy low allows film growth at low temperatures and high growth rates. Using fluorinated gas (SiF_4 and H_2) mixture, device quality poly Si films (grain size of > 100 mm, (2 2 0) or (4 0 0) orientation and an electron mobility of

$\sim 13\,cm^2/V\,s$) have been achieved at a deposition rate of ~ 1.5 nm/s by remote-type microwave PECVD, at a growth temperature of less than 400°C [39].

Jones et al. [40] used a gas jet technique to deposit μc-Si at a rate of 2.0 nm/s. In this approach, a high-speed gas stream is subjected to microwave excitation which decomposes it, forming a plasma close to the gas jet nozzle. After the decomposition, radicals, ions and neutral species generated in the plasma quickly reach a heated substrate surface, due to the high-speed gas flow. The use of microwaves allows high silane decomposition rates and a large amount of hydrogen etching of the film growth surface, as required for microcrystalline film formation. The materials had a grain size of 20 nm, and were found to have some regions that were columnar in nature and others that did not have a preferentially oriented microstructure. The low-pressure (mTorr) regime minimises the gas phase interactions and possible multihydride Si radical formation that are causes of powder formation. Using a linear microwave plasma source, μc-Si has been obtained at a growth rate of > 1 nm/s [41]. Homogeneous deposition on a large area is reported.

A high-density microwave plasma [42] obtained using a spokewise antenna was employed to produce microcrystalline films from SiH_4 (without hydrogen dilution and applying silane depletion and low pressure) at a growth rate of 4.7 nm/s and a low substrate temperature of 250°C. The plasma maintains a high electron density of $n_e > 10^{11}\,cm^{-3}$ and a low electron temperature T_e of 2–2.5 eV. Addition of hydrogen to the source gas decreases the defect density, and a photosensitivity of 100 has been achieved for a material that is intrinsic in nature [43]. A low defect density of $5 \times 10^{16}\,cm^{-3}$ is reported for polysilicon films grown at a rate of 4.7 nm/s (random orientation) from a gas mixture $SiH_4/H_2 = 30/30$ [10]. The method also claims the ability to maintain plasma homogeneity over a large area of 22 cm diameter. Films with a preferred orientation (2 2 0) can be made at 2.0 nm/s with a defect density of $2.5 \times 10^{16}\,cm^{-3}$. A high SiH_4 flow rate, a higher pressure and a lower temperature showed a reduction in the defect density.

Shinda et al. [44] obtained a high plasma density ($> 10^{12}\,cm^{-3}$) and a very low electron temperature (< 1 eV) by microwave excitation (8.3 GHz) using a radial line slot antenna (RLSA). This can be compared to the $10^{10}\,cm^{-3}$ plasma density and several electron volts electron temperature obtained in the case of PECVD. Using a gas mixture of SiH_4/Xe (1:30) without hydrogen dilution, it is possible to deposit poly Si films (20 nm grain size) at a low temperature of 300°C and a deposition rate of ~ 2 nm/s. This has been attributed to the low energy (~ 3 eV) ion bombardment, the high flux ion irradiation and the large mass and radius of the Xe^+ ion bombardment. The importance of the Xe^+ ions is due to (i) a large mass, resulting in more effective bombardment, (ii) a low penetration probability into the silicon lattice due to the large radius, resulting in less damage to the silicon crystal and (iii) a much lower ionisation potential than for silane.

2.2. *Ion free depositions*

In the previous section, we saw that the suppression of ions reaching the substrate and a lowering of the ion impact is one of the key parameters for μc-Si deposition. It

will be more favourable if the gas chemistry does not involve ions. Below are some of the cases in which the deposition species are neutral (radicals).

Photo-CVD: In photo-CVD deposition, photons are used to dissociate the process gas. There are two methods for achieving this: direct and sensitised. In the latter case, sensitisers such as mercury atoms, excited by UV radiation, transfer energy to the process gas and dissociate it ($Hg^* + SiH_4 = Hg + SiH_3 + H_2$, $Hg^* + H_2 = 2H + Hg$). As the photons do not have sufficient energy to ionise, the species generated through dissociation are radicals. Mercury-sensitised photochemical vapour deposition (Photo-CVD) from a $SiH_4 + H_2$ gas mixture resulted in microcrystalline silicon films, grown at a high rate of 0.05 nm/s and having a photosensitivity of 550 [45]. However, such relatively good material properties have not been translated into device performance.

ETP: In the ETP process, the thermal plasma created in an Ar and hydrogen mixture expands into a low-pressure chamber where atomic hydrogen reacts with injected SiH_4 and the plasma transports the created radicals to the substrate. There is a significant contribution of reactive radicals such as SiH_x ($x < 3$) (SiH (2%) and Si (0.2%)) to growth, though 90% of it is due to SiH_3. This deposition process is considered here as ion free because the fraction of ions reaching the substrate surface is small. This technique has been used to deposit μc-Si at a growth rate of 2.7 nm/s [24] and a substrate temperature of 250°C. This is attributed to a high atomic hydrogen flux ($\sim 1.5 \times 10^{12}\,cm^{-3}$ in the absence of silane), in the conditions for microcrystalline growth. A grain size of 20 nm, a photosensitivity of 100 and a DC conductivity activation energy of 0.6 eV show the device quality.

HWCVD: In HWCVD, silane molecules catalytically crack above 1500°C, in the presence of heated filaments, into Si and H atoms i.e., $SiH_4 = Si + 4H$. The other reaction is $H_2 = H + H$. However, for poly Si deposition, these species do not reach the surface but rather go through gas phase reactions. Hydrogen reacts with silane to create radicals $H + SiH_4 = SiH_3 + H_2$ and the main species SiH_3, along with abundant atomic hydrogen facilitates poly Si growth. On the other hand, Si is lost in a gas phase reaction: $Si + SiH_4 = Si_2H_4^*$. Alhough electron emission from filament can lead to ionised species, the effect is negligible.

After the report by Matsumura [46] on poly Si deposition by HWCVD ((2 2 0) oriented grains, at a substrate temperature below 450°C), many reports on poly Si deposition have been made by various groups. Matsumura [47] showed that films with an electron mobility above 20 $cm^2/V\,s$ could be achieved. Cifre et al. [48] showed that poly Si ((2 2 0) oriented) could be made at a temperature as low as 280°C and a deposition rate as high as 3.7 nm/s The substrate to filament distance can be used as an optimizing parameter. Deposition of poly Si at a high growth rate, either by using a shorter substrate to filament distance [49] (4.0 nm/s at $T_s = 300$°C) or multiple wires [50] (1–5 nm/s at $T_s = 500$°C), and the capability for n- and p-type poly Si deposition by these processes opened up the possibility of a promising deposition method for poly Si solar cells. However, it was the poly Si deposition at Utrecht University by Rath et al. [51] which showed that a device quality intrinsic poly Si layer can be made, which satisfies all the opto-electronic requirements (see Table 1) for solar cell applications. The first working solar cell, with 3.15% efficiency

Table 1
Physical properties of device quality poly Si material made by HWCVD at Utrecht University (Rath et al. [51])

Material properties	
Cryst. Vol. Frac. (%; Raman)	95
Average grain size (XRD) (nm)	70
Dep. rate (nm/s)	0.55
H content (at%)	0.47
Diffusion length (SSPG) (nm)	568
σ_{ph} ($\Omega^{-1}\,cm^{-1}$) (100 mW/cm^2 AM1.5)	2×10^{-5}
σ_d ($\Omega^{-1}\,cm^{-1}$)	1.5×10^{-7}
Band gap (eV)	1.1
Activation energy (eV)	0.54
Defect density (ESR) (cm^{-3})	7.8×10^{16}
Activation energy (eV) (Hall mobility)	0.012
Roughness (AFM) (nm)	150
SIMS (oxygen content)	$\sim3\times10^{18}$/cm^3
IR (oxygen in the film)	Very low

Table 1

(deposited on n^+c-Si surface), was presented. This was followed by a real thin film solar cell on an SS substrate, showing an efficiency of 4.41% [52]. These extensive studies identified the effect of deposition parameters on the structural and opto-electronic properties. Hydrogen dilution mainly affects the structure; the orientation changes from random at high hydrogen dilution to exclusive (2 2 0) orientation at low dilution. High pressure mainly increases the deposition rate at the cost of defect density, though without much effect on the structure. It is the wire temperature (T_{fill}) which defines the electronic properties, and a T_{fill} value of 1800–1850°C was identified as the regime for achieving device quality poly Si. As will be discussed in the other sections of this article, poly Si films with large columnar grains forming a compact structure, an exclusive (2 2 0) orientation of grains, a very low oxygen incorporation and an intrinsic nature have been made by this technique.

The role of the chamber walls on crystallinity has also been reported. Komoda et al. [53], using $SiH_4/H_2 = 5{:}50$ sccm at a substrate temperature lower than 300°C, obtained poly Si ($V_f > 90\%$) at a deposition rate of 1.1 nm/s and a low defect density of $2\times10^{16}\,cm^{-3}$. The defect density increases with deposition rate (with higher pressure). High order silanes formed by reaction with the Si deposited on the walls deteriorate the crystallinity, and cleaned chamber walls give films with lateral grain sizes as high as 500 nm.

Matsumura [54] showed that though poly Si can be easily made by HWCVD using H_2 diluted silane, even at temperatures below 400°C, with a proper deposition regime, such films could be made even from pure silane. Increasing the pressure is the easiest way of achieving crystallinity, in addition to increasing the deposition rate. Konagai et al. [55] also found that in a hot-wire CVD process, poly Si is obtained at high gas pressures, though in their case the filament configuration, called a "hot wire cell", is different (perpendicular to the substrate surface). This is attributed to a preferential supply of SiH_3 and a sufficient supply of atomic hydrogen in the

high-pressure regime. Poly Si films can be made without hydrogen dilution ($T_s = 175-400^\circ C$) if the filament temperature is between 2000°C and 2100°C. At low filament temperatures (1700–1900°C), amorphous silicon films are formed. The crystal orientation depends very much on the filament and substrate temperatures. A maximum deposition rate of 3 nm/s was obtained by this method. The best poly Si (hydrogen content 2–3%) obtained by this method [55], at $T_s = 250^\circ C$, had a photosensitivity of ~ 100 and a dark conductivity of $\sim 10^{-7}\,\Omega^{-1}\,cm^{-1}$. The high deposition rate which was achieved while maintaining a low substrate temperature was attributed to the "hot wire cell" allowing a more efficient catalytic reaction of the gas with the filament (the reactant gas is decomposed effectively while travelling through the filament) and to a low value of heat radiation to the substrate. Moreover, sufficient atomic hydrogen supplied from the SiH_4 decomposed at the filament allows for poly Si growth without hydrogen dilution. The TIT group also obtained epitaxial Si [56] at 200°C, using this method of deposition.

The filament material and temperature have a significant role in achieving crystallinity. Bruhne et al. [57] reported that with the new filament from MVSystems (USA) they obtained amorphous films at $T_s > 450^\circ C$, whereas with W and Ta filaments predominantly poly Si is obtained at these temperatures. At $T_s = 320^\circ C$, films showed an exclusive (2 2 0) orientation, with a 40–45 nm grain size and less strain in the grains. The photoluminescence showed no contribution from the band tail, and it is tempting to correlate this with the (1 1 0) oriented growth. Lee et al. [58] observed (for a 0.5 mm diameter, 7 cm coiled W wire) that the filament temperature has a big role in determining the crystallinity. At $T_{fill} = 1800^\circ C$, a crystalline volume fraction, V_f, of 70%, with randomly oriented grains, is observed. However, at $T_{fill} = 2000^\circ C$, the film has $V_f = 91\%$, and a (2 2 0) preferential orientation (when the comparison was made at the same substrate temperature). They observed that at high filament temperatures there is no significant variation in microcrystallinity with hydrogen dilution, and even films made without hydrogen dilution are poly Si.

The combination of HWCVD with other deposition techniques has also been tried, and looks promising. RF-assisted HWCVD or hot-wire-assisted PECVD is used to take the separate advantages of the HWCVD and PECVD processes. In such an approach, Feng et al. [59] saw an improvement in V_f (93%), deposition rate, and (2 2 0) oriented grains when a high T_{fill} is used ($T_s = 300^\circ C$, wire: tungsten, PECVD: 13.56 MHz, wire inside the parallel plate capacitor). However, Ito et al. [60], with a different configuration (filaments perpendicular to the RF electrodes), saw no dramatic changes in crystallinity or defect density when introducing an RF assembly to the HWCVD process. However, a decrease in the deposition rate was observed. A combination of VHF PECVD and HWCVD [61] leads to a deposition rate as high as 2.6 nm/s, without powder formation, for μc-Si obtained while maintaining a defect density similar to that of a film made by standard VHF at low deposition rates. Dalal [62] has proposed combining HWCVD with ECR to get high deposition rates.

One of the novel ways to increase the deposition rate is to combine HWCVD and sputtering techniques [63]. The method uses the principle that the etching rate of Si by atomic hydrogen depends on the temperature of the Si target. Atomic hydrogen generated by the HWCVD process reacts with a Si target, and the generated SiH_4

species are chemically transported towards the catalyser. The generated SiH_4 molecules are catalytically decomposed by the heated catalyser and a poly Si film is deposited on substrate. The cooled Si target allows for efficient etching, whereas the higher temperature of the substrate suppresses etching by hydrogen, thereby facilitating the deposition. By this method, called chemical sputtering (though in principle it is a chemical transport technique), large grains of size 1 μm have been obtained at $T_s = 400°C$ for a poly Si film about 1 μm thick. Reduction of the Si_2H_6 species was considered to be one of the causes for the large grain size. Deposition seems to be selectively possible on a Si substrate. For a quartz glass substrate, a seed poly Si layer deposited by conventional method (HWCVD) is necessary to deposit poly Si by chemical sputtering.

A deposition process, similar in concept to HWCVD, uses a hot plasma column instead of a hot filament. The process employs a higher gas temperature in the plasma, leading to a higher dissociation rate, a higher radical production rate and a high deposition rate. A DC discharge is maintained between a heated tungsten filament cathode and a water-cooled copper anode, 50 cm apart. The technique, called DC plasma CVD [64], also has the advantage of providing a powerful source of atomic hydrogen, beneficial for microcrystallinity. Preferential (2 2 0) oriented films are made at a high hydrogen flux ((1 1 1) oriented films are made with a silane–argon plasma). A deposition rate of 10 nm/s has been achieved at a deposition temperature lower than 450°C. Microcrystalline films were obtained even without H dilution, due to the high dissociation efficiency of silane leading to a large atomic hydrogen concentration.

2.3. Sputtering

Ion-assisted sputter deposition (pulsed-DC magnetron) in an Ar atmosphere gives a deposition rate of unhydrogenated microcrystalline silicon of 1.5 nm/s at temperatures of 400–500°C [65].

2.4. High temperature depositions

We present here some recent reports of high temperature poly Si produced by CVDs, to compare them with those produced under low temperature depositions (with respect to deposition rates). An extremely high deposition rate of 1000 nm/s has been reported for microcrystalline silicon deposition by an ultra fast approach called DC-RF hybrid thermal plasma chemical vapour deposition (DC-RF TPCVD) [66]. However, the defect density is high $\sim 10^{17}/cm^3$, even using a two-step process (a low rate deposition in the initial stage followed by a high rate deposition). Wang et al. [67] deposited a poly Si layer by an atmospheric pressure iodine vapour transport technique at a substrate temperature of 900°C. Films with grain sizes of 20 μm, with a (1 1 0) preferred orientation, were made at a high deposition rate of 50 nm/s. They showed a hole Hall mobility of $51\,cm^2/V\,s$ at a doping density of $5.5 \times 10^{17}\,cm^{-3}$, and $76\,cm^2/V\,s$ after hydrogen passivation. TEM pictures showed that the grain boundaries were conformal, and stacking faults and twins (which are believed to

have a minimum impact on solar cell performance) with occasional dislocations were the major defects. However, the Raman peak shows a shift of $3\,cm^{-1}$ from the ideal c-Si position, indicating stress in the material. HIT cells with these poly Si layers showed open circuit voltages (V_{oc}) of 0.48 V and 0.58 V at one sun and 13 suns, respectively, which was attributed to the (1 1 0) structure. More information on the effect of the (2 2 0) oriented structure on solar cell performance is presented in Section 4.2.

3. Technological challenges

3.1. Growth rate

One of the characteristics that play a decisive role in the suitability of any deposition process for device application is the deposition rate. Maintaining device quality while increasing the deposition rate is a challenge to materials researchers. In PECVD, source gas (SiH_4) preheating (cathode heating) [68] can be employed to improve crystallinity. Improvement of homogeneity and crystallinity in the early stages of growth at a cathode temperature $T_c \geqslant 550^\circ C$ and $T_s = 180^\circ C$ has been demonstrated. This method can have a beneficial effect on reducing powder formation in the case of samples deposited at a high rate by techniques such as HPD. The substrate temperature plays a significant role in determining the microcrystallinity, and may influence the growth rate in addition to the crystalline volume fraction, grain orientation and size. Matsuda [9] reported that the deposition rate monotonically (but slowly) increases with increasing temperature, though there is an optimum temperature of 300–350°C for obtaining a maximum crystalline fraction. However, this effect has been contested by Veprek et al. [8] who showed that crystallinity increases monotonically with increasing T_s up to $>500^\circ C$, if impurities can be avoided. We assess here the microcrystalline films made by various deposition techniques (the best results obtained by various laboratories) discussed in the last section. Fig. 1 shows the deposition rate versus the substrate temperature. From the figure, it is seen that there is no clear dependence. For low frequency PECVD or ion-less depositions, a trend of high growth rates at high substrate temperatures can be obtained. However, higher frequencies, or ion-assisted depositions allow a high growth rate at lower substrate temperatures. It can be summed up that there are varieties of deposition parameters which influence the deposition rate, and substrate temperature is only one of them (not necessarily the most dominant one).

3.2. Incubation

Microcrystalline silicon deposition is an inhomogeneous growth process. The deposition generally begins with an amorphous phase. It needs a minimum thickness called the incubation phase before a localised phase transformation takes place, which is called nucleation. Although the exact mechanism of nucleation (physical

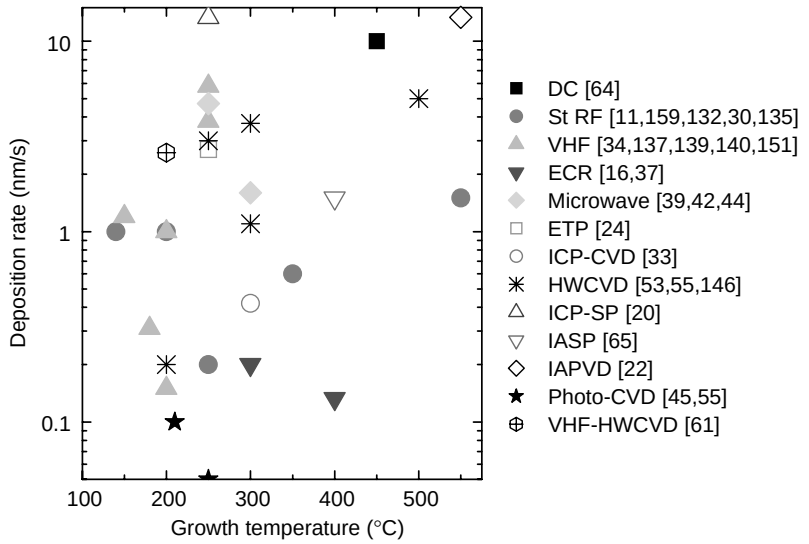

Fig. 1. Deposition rate of microcrystalline films at various substrate temperatures, for different deposition techniques.

reason) is still not understood, the dynamics of the phase transformation have been monitored by various techniques, and various models for the nucleation process have been proposed. Once a nucleation has occurred, the crystals grow around this. Zhou et al. [69] have shown that μc-Si with complete elimination of the amorphous incubation phase can be obtained by employing a triode system in a PECVD process (13.56 MHz), with a high hydrogen dilution of the silane gas mixture. High crystallinity in the film (deposition rate of 0.2 nm/s) was obtained up to a small thickness of 6 nm, and there was ample evidence that even at a 2 nm thickness, crystallites are already formed in the film. The rapid nucleation was attributed to a drastic reduction of ionic bombardment in a triode system, when a negative voltage is applied to the mesh. Ion bombardment is considered to retard nucleation, as discussed in Section 2.1.1. In order to make microcrystalline films at high deposition rates without an incubation phase, a two-step deposition process is applied. One approach is to change the temperature from the first initial step of short period deposition (seed layer) to the second step of longer period deposition [70]. Heya et al. [70] employed a seed layer (200 s of deposition) made at a high substrate temperature (no incubation at the high substrate temperature) and a second step (800 s of deposition) at a low substrate temperature. In this manner, it is possible to make microcrystalline films by keeping the substrate at high temperature for a reduced period of time, and most of the deposition can be made at a temperature below 400°C. Two-step growth [71,72] has also been utilised to improve microcrystallinity in microwave plasma deposition. The first layer can be a poly Si film made at 360°C and/or by a layer-by-layer (LBL) technique. In the second step, epitaxial-like growth of poly Si can be carried out at a temperature <320°C.

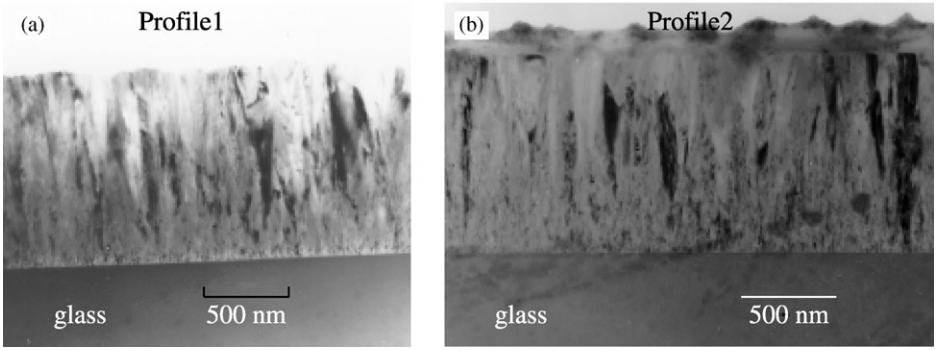

Fig. 2. Cross-sectional electron microscope images of profiled layers made by HWCVD at UU [73]. Poly1: high hydrogen dilution, Poly2: low hydrogen dilution: (a) Profile 1: Poly1(20 nm)/Poly2, (b) Profile 2: Poly1 $\xrightarrow{H_2 \text{ dilution decrease}}$ Poly2.

Another two-step process is to change the hydrogen dilution between the two steps of deposition [69,73]. For the case of RF PECVD [69], the first step is the deposition/formation of a seed layer at $SiH_4/H_2 = 0.33/99$ sccm. On top of this, the second step is growth at $SiH_4/H_2 = 1.2/99$ sccm, which gives a higher deposition rate. For the case of HWCVD, the concept of profiled layers (to get rid of the incubation phase) has been proposed [73]. There are two processes for achieving this. In the first, a compact poly Si (called Poly2, made at a low hydrogen dilution of silane gas) is deposited on a seed poly Si layer (called Poly1, made at a high hydrogen dilution). In the second type of profiled layer, the hydrogen dilution was continuously varied from high to low, and thus the material changes from Poly1 to Poly2 continuously. Fig. 2 shows the cross-sectional transmission microscopy (XTEM) of the two types of profiled layers [73].

Wang et al. [74] reported that by introducing hydrogen dilution downstream in an RF excited remote PECVD, the deposited films showed no detectable transition amorphous layer between the substrate and the deposited microcrystalline silicon film, for T_s from 350°C down to 100°C. This shows a way to avoid an incubation phase. Bouree [75] (HWCVD: W wire, T_s: 230°C, $T_{fill} = 1500$°C) observed from ellipsometry studies (similarly to the earlier report by Rath et al. [73] from TEM studies) that at a high hydrogen dilution of 98%, the film is microcrystalline (30 nm crystallites), without any incubation layer. However, it contains a high void fraction, whereas at a low dilution of 94%, the material is microcrystalline with a low void fraction (8%), but contains a 17 nm thick incubation amorphous layer. They followed a technique similar to that proposed by Rath et al. [73], where the dilution was varied during the deposition, from an initially high to a finally low value. Films made by this "variable dilution" process are microcrystalline, with a low void fraction (10%) and a low amorphous fraction, but without an incubation layer.

The observation that a continuous plasma between the seed layer and the subsequent growth is not needed suggests that a variety of techniques can be applied to achieve rapid nucleation (as a seed layer) and a completely different growth

method can be subsequently applied on top of it [69]. An example is a seed layer prepared by SPC, LBL or laser annealing [76], followed by a microcrystalline film deposited at a high growth rate by PECVD.

Several combinations of PECVD with other processes have been tried, seeking to influence the initial growth. This is an effective way to avoid the incubation phase in a one-step deposition process. One such approach is excimer laser (308 nm wavelength) assisted RF glow discharge deposition ($SiH_4 + He$ gas mixture, deposition rate of 0.2 nm/s) in which laser annealing was performed during deposition [77]. At a laser fluence higher than a critical value (165 mJ/cm^2), microcrystalline films were formed at 250°C, which showed a high electron mobility (60 cm^2/V s) and an optical absorption coefficient ten times higher than that in c-Si.

3.3. Lowering the growth temperature

For the application of microcrystalline films on flexible plastic substrates, and to avoid incorporation of impurities from substrates and underlying layers, the process temperature has to be significantly reduced. Here, some of the cases in which films have been deposition below 150°C are presented. This allows for the use of some types of plastic substrate.

The growth temperature can be significantly reduced by using halogenated silane. This has been shown with the use of chlorinated silane source gases such as SiH_2Cl_2, $SiHCl_3$, and $SiCl_4$ with hydrogen dilution [78]. The dilution of $SiF_4 + H_2$ in the plasma with He gas is shown to improve crystallinity and entirely microcrystalline films have been made by PECVD at a low substrate temperature of 120°C [79].

Ion suppression is an important step to lower the growth temperature. Application of a positive bias to the substrate in an ECR CVD deposition has shown that it is possible to deposit poly Si films on polyethylene terepthalate (PET) (maximum service temperature 150°C) and polyethersulfone (PES), (maximum service temperature 200°C) substrates [80].

A high atomic hydrogen flux in the plasma is also an effective way of obtaining crystallinity at a low substrate temperature. Alpuim et al. [81] looked at depositing microcrystalline silicon at a low substrate temperature (250–25°C) by RF-PECVD and HWCVD. They observed that the deposition rate is independent of T_s. In RF PECVD, more hydrogen dilution is needed for the amorphous to μc-Si transition at low T_s. However, in HWCVD the dilution is independent of temperature for such a transition, which has been attributed to the high atomic hydrogen flux in HWCVD. The other difference is that the transition is abrupt for RF deposited films (within an interval of 1–2% of dilution) whereas the transition is gradual (dilution between 80% and 90%) for the HWCVD case. The parameter range for the deposition of μc-Si is seriously reduced in the case of RF PECVD, upon reducing the substrate temperature.

The nucleation seems to depend on the type of deposition process, and this has a consequence on the influence of substrate temperature on crystallinity. For example, it is proposed that in the case of RF PECVD, the nucleation of crystallites is preceded by the formation of a highly porous, protocrystalline film. On the other

hand, in the case of HWCVD, small highly ordered regions, normally present in amorphous silicon films, are the origins of crystallites at high dilution, without the need for the formation of a porous nucleation layer as in RF. μc-Si films with a crystalline fraction $>80\%$ have been obtained for HWCVD deposition independent of T_s, whereas in the case of RF-PECVD the crystalline volume fraction decreases strongly with reduced T_s.

4. Physical properties

4.1. Defects

Microcrystalline and poly silicon, being multiphase materials (crystalline grains, amorphous tissue, grain boundary), the types of defects, their locations and participation in the recombination process have still not been properly analysed. However, in recent years, a number of defect studies have resulted in a wealth of data on defect states in these materials. The interpretation of sub-bandgap absorption spectra by the constant photocurrent method (CPM) and photothermal deflection spectroscopy (PDS), for defect characterisation, has not been well established. This is due to the lack of understanding of the density of states (DOSs) and the optical transitions. Electron spin resonance (ESR) is one technique that has given a lot of useful data, based upon which the DOSs picture can be worked out. Fig. 3 shows an example of the ESR spectra of intrinsic μc-Si made by HWCVD. Details of the spectra in this figure will be discussed later in this section.

Information about the DOSs and (particularly) the tail states can be obtained by shifting the Fermi level continuously using various types of p-type and n-type doping. In such a detailed study, Finger et al. [82] found that microcrystalline silicon contains two types of mid-gap defect. One of them, with $g = 2.0052$, is attributed to dangling bonds (dbs) at the column boundaries. This g value is slightly lower than the db line in amorphous silicon, but it has the same line width, spin-lattice relaxation time, temperature dependence and increase of intensity with electron irradiation. However, many reports on poly Si made by a wide variety of techniques such as VHF PECVD [83], HWCVD [84] and SPC [85] identified silicon db centres at the same g value as that for amorphous silicon, i.e., $g = 2.0055$. These db centres are randomly oriented defects in a microcrystalline structure, like the randomly oriented db defects in amorphous silicon. However, a number of other types of db defect centres associated with the special grain boundary properties have been identified. They are namely the anisotropic P_b type centre with $g = 2.006$ [86,26], and the anti-ferromagnetically coupled db pair at $g = 2.005$ [84]. In addition to these intrinsic defects, impurity-related db centres are also reported. A centre at $g = 2.0043$ has been related to dbs in oxygen-rich regions [82,87]. Another centre at $g = 2.0026$ [83,86], considered to be oxygen related, has also been detected. The origin of this has been ascribed to oxygen contamination in the chamber, which leads to defect centres like those in SiO_2 [86] and the existence of this centre is ambient dependent [83]. Upon annealing μc-Si to high temperatures, Vanecek et al. [83] observed not

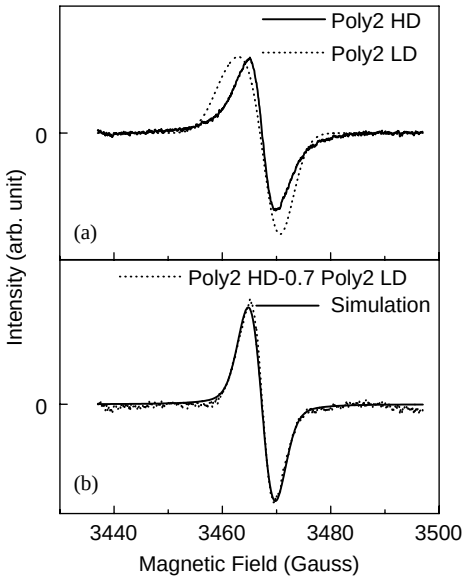

Fig. 3. ESR spectra of HWCVD poly Si films [84]. Both the films have the same structure ((2 2 0) oriented): (a) Poly 2LD: low defect density, Poly2HD: high defect density; (b) the spectrum after subtraction of the contribution of Poly2LD from Poly2HD.

only an increase in the concentration of the db defect centres at $g = 2.0055$, but also the creation and growth of another centre around $g = 2.003$. Alhough they differentiate this centre from the other species with $g = 2.0026$ which is ambient dependent, it would be safe to suggest that this $g = 2.003$ centre could be also generated due to the interaction of contaminants with the grain boundaries.

Proper resolution of ESR spectra is necessary to accurately identify the different centres in a complex ESR spectrum. Ehara et al. [86] studied ESR in unhydrogenated μc-Si deposited by RF sputtering. Experiments in the X and Q bands distinctly resolved the two types of centres. One is a defect centre with a g value at 2.006, and there is a narrow line at 2.0026. The former, which showed considerable anisotropy ($g_{\parallel} = 2.002$, $g_{\perp} = 2.008$) has been attributed to the so-called P_b type centre. The $g = 2.006$ centre was also observed in plasma CVD μc-Si, whereas that with $g =$ 2.026 was absent. The P_b centre has also been observed by other groups, for the case of plasma CVD grown μc-Si [26].

Kondo et al. [26] showed that for (2 2 0) preferential oriented μc-Si deposited by RF PECVD, the db defects show considerable anisotropy when the magnetic field is parallel or perpendicular to the substrate. Instead of interpreting the broadened line in terms of deconvoluted lines from different centres, it was suggested that the anisotropy could explain the broadening of the line. Three contributions to the ESR line have been considered, (i) an anisotropic component with $g_{\parallel} = 2.0023$ and $g_{\perp} =$ 2.0078, attributed to the P_b centre with axial symmetry, situated at the grain surface of the (2 2 0) oriented grains, (ii) a powder-like component, attributed to dbs at the

grain boundaries of the randomly oriented small grains, (iii) an isotropic component from the a-Si:H matrix. Effusion of hydrogen at 400°C shows a simultaneous increase in the anisotropic component, due to desorption of hydrogen from the grain boundaries. Effusion at 600°C increases the isotropic component due to desorption of hydrogen from the amorphous matrix.

Vanecek et al. [83] found a good correlation between the height of the CPM spectrum at 0.8 eV and the ESR signal at $g = 2.0055$; the relation being that a defect density of $2 \times 10^{16}\,\mathrm{cm}^{-3}$ corresponds to $\alpha(0.8\,\mathrm{eV}) = 0.12\,\mathrm{cm}^{-1}$.

As far as tail states of μc-Si are concerned, the data are inadequate to draw any conclusions concerning the DOS at the band edges. The $g = 1.996-1.998$ line, sometimes observed in intrinsic microcrystalline silicon, is clearly observed in n-type films [82]. A clear correlation between the dopant density, the free carrier (n_{Hall}) density and the conduction electron (CE) spin density is observed. It has been proposed that structural disorder leads to localised tail states and the conduction band tail states overlap the donor states (P_4 states in phosphorus-doped material; a weak hyperfine structure has been identified). The CEs are distributed in the tail states, dopant states and extended states. With increasing temperature, the electron distribution shifts towards the band edge. As far as the valence band tail states are concerned, a line with $g = 2.01$ observed in boron-doped films has not been assigned.

Because of the proximity of the dbs in a thin grain boundary region, various exchange interactions between defects take place. The study of the line width provides information about the location and orientation of defects at the grain boundaries. Nickel and Schiff [85] studied, by ESR, db defects in solid phase crystallised poly silicon films with and without hydrogen passivation. A single db ESR line ($g = 2.0055$) inhomogeneosly broadened due to randomly oriented defects was observed. The temperature dependence of the ESR signal shows very interesting results. The g value and spin density showed no temperature dependence. However, the line width showed a monotonic decrease with increasing temperature, which was attributed to motional narrowing. The line width is given by the relation

$$\Delta H_{\mathrm{pp}}(T) \approx \Delta H_0/(1 + \nu_{\mathrm{H}} T_1),$$

where T_1 is the spin lattice relaxation time, ΔH_0 is the low temperature line width, and ν_{H} is the hopping rate given by $\nu_{\mathrm{H}} = \nu_0 \exp(-E/kT)$, where T is the temperature and E is the energy barrier for hopping. This relation adequately simulated the experimental temperature dependence of the line width. Two possibilities for hopping have been proposed: diffusion of the db centre and exchange of the electron of a hydrogen atom between a pair of defect sites.

Rath et al. [85] observed a different kind of spin exchange interaction in their poly Si films. The ESR spectra of HWCVD deposited device quality poly Si films ($N_{\mathrm{d}} = 7.8 \times 10^{16}/\mathrm{cm}^3$) show only an inhomogeneously broadened single line at $g = 2.0055$, with a peak-to-peak line width (ΔH_{pp}) of 7.6 G (Poly2 LD, Fig. 3a). This broad line from the low defect sample is due to isolated defects with a g-tensor anisotropy, with diagonal elements $g_{xx} = 2.0040$, $g_{yy} = 2.0040$, $g_{zz} = 2.0090$.

However, for films with a higher defect density (Poly2 HD, Fig. 3a) with the same (2 2 0) oriented structure, the line width shrinks. A computer simulation of the narrowed ESR line of Poly2 HD shows that there are two contributions, i.e. (i) a broad line as found for the low defect density materials and (ii) a Lorentzian narrow line with $g = 2.005$ and $\Delta H_{pp} = 5\,G$ (Fig. 3b). There are two types of spin system in the material. The temperature dependence of the magnetic susceptibility, χ, shows that there are two contributions: (i) isolated defects (dbs) which follow simple Curie behaviour and (ii) paired spins experiencing anti-ferromagnetic coupling with a Weiss temperature of $-136.4°K$. The exchange coupling energy, J, in the interaction between the two spins in the dimer ($E = -J\mathbf{S_1} \cdot \mathbf{S_2}$) is estimated to be 9.91 meV. This exchange interaction between defects in the dimer is of Heisenberg type. It has been proposed [84] that there are regions at the grain boundaries where the defects are clustered. Thus, defects can be sufficiently closely spaced to allow exchange interactions. The constraints imposed by exclusively (2 2 0) oriented material and the compact structure facilitates such interaction between oppositely oriented defects along the (1 1 1) axis. The poly Si:H films thus appear to have such a highly compact structure that the defects have to be accommodated in the narrow region between columns, and have a tendency to form defect pairs.

The electronic defects in microcrystalline silicon can also be observed by spin-dependent transport properties. By such experiments, the defects and recombination processes involved in a carrier transport path can be identified. This information is very important for μc-Si in device applications, because not all defects have an adverse effect on the electronic processes in devices. In an experiment such as electrically detected magnetic resonance (EDMR) or spin-dependent photoconductivity (SDPC), the resonant change of the sample current is observed. This occurs when the sample is brought into magnetic resonance. For the observation of these effects, it is essential that spin selection rules determine the transition rate between the participating localised states, which are paramagnetic. From EDMR studies, Stutzmann et al. [88] assigned the $g = 2.005 \pm 0.005$ to db types of centre.

While studying defects and recombination by ESR and EDMR in PECVD microcrystalline films by stepwise annealing from 200°C to 750°C Will et al. [87] revealed that there are three kinds of defects, $g = 2.0055$ (db), $g = 2.0044$ (oxygen-related) and $g = 1.998$ (CE), and that most of the defects are distributed at the column surfaces. They concluded that electronic transport is not controlled by defects, if the defect density is $N_D < 10^{18}\,cm^{-3}$. Here, it is attributed to conduction through percolation paths. However, for $N_D > 10^{18}\,cm^{-3}$, hopping conduction through the grain boundaries is identified. One interesting observation by these authors is that oxygen incorporation does not influence the electronic properties, because of either a simultaneous increase in the defect density or the specific location of defects at columns.

The spin-dependent process shows the property of the CE centre and its role in recombination along the transport path. The CE line [88] at $g = 1.998$, which sometimes appears in the dark and always appears with illumination, has been attributed to electrons in shallow traps around the microcrystals. Upon illumination,

spin-dependent recombination between these shallow electrons and the dbs has been identified. A similar observation was also made when comparing ESR (in the dark) and light-enhanced spin resonance (LESR), where an increase in both the $g = 2.0055$ and the $g = 1.998$ line occurred with illumination.

While studying a series of HWCVD microcrystalline films, Kanschat et al. [89] observed that the $g = 1.998$ line intensity increased with increasing illumination. However, they found a weak dependence of these CE centres upon the carrier generation rate (G) under illumination ($\Delta N_{CE} \propto G^{\gamma}$, where $\gamma = 0.16$). This is similar to the variation of the concentration of electrons in the localised states in a-Si:H, instead of a linear dependence as generally observed for the dependence of the photoconductivity upon the generation rate. Thus, they attributed the CE states to shallow localised states below the conduction band edge. From SDPC studies, the spin-dependent recombination process at low temperature has been attributed to a transition (tunnelling) from a CE state to a neutral db (CE-db), which is a dominating recombination channel at temperatures below 50°C. Above 50°C, the transport changes from hopping in the band tail to band conduction, and the CE signal disappears. It is suggested that disorder at the grain boundaries leads to band tails in poly Si films, and the CE resonance is attributed to intrinsic tail states which are probably located at the grain boundaries. The presence of such tail states is confirmed by other reports [90].

Fig. 4 shows the DOS of microcrystalline material, based upon currently available data. There is not much information on the width of the conduction band tail. The energy positions of the various mid-gap states have also not been evaluated. The recombination process through the db ($g = 2.0055$) has been established. The participations of other mid-gap centres, especially the impurity (oxygen)-related ones, have not been established.

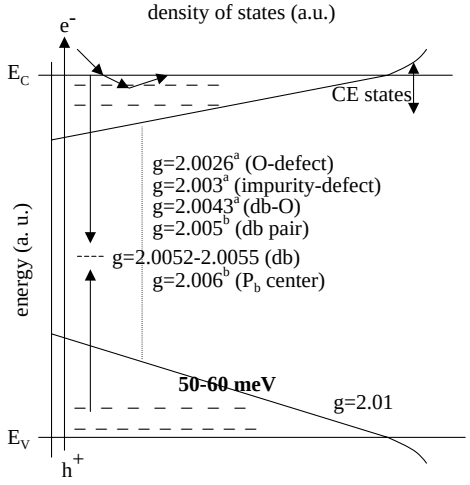

Fig. 4. DOSs of microcrystalline silicon material.

4.2. Structure

A great amount of work has been done in recent years on the structural study of poly crystalline films, from which a relation between structure and solar cell efficiency has been obtained. Two groups have conducted extensive work on this, and have come to similar conclusions. The Julich group [91,92] obtained poly Si with a grain size of 50 nm for a material grown at 200°C at 2% silane concentration. Three regimes of growth have been identified: (i) at high hydrogen dilution, where there is highly crystalline growth with crystal columns extending throughout the film, (ii) near the transition to amorphous growth, where the crystal columns are smaller and there is a considerable fraction of disordered material between the columns, (iii) predominantly amorphous growth with small crystallites embedded in an amorphous matrix. A significant observation is that it is not the highly crystalline regime (region (i)) that gives the good solar cell performance. Rather, it is the material in the transition regime (region (ii)), which shows the highest efficiency. The possible reason for a material with a significant disordered phase to give the best performance could be that in that case the grain boundaries are passivated by hydrogen. Unlike other reports, the Julich group finds that crystalline growth starts at nucleation centres near the interface between the film and the substrate, and grows in a conical shape. After a certain stage, the columnar structure evolves with stable grain boundaries between the columns, and the grain size becomes independent of thickness.

Vallat-Sauvain et al. [93] from IMT (Neuchatel group) showed schematically the changes in microstructure with the silane to hydrogen ratio. Samples close to the phase transition show elongated nanocrystals embedded in an amorphous matrix. At intermediate dilutions, a dendritic growth is observed, and at high dilution samples have a columnar growth. It is for the films grown at intermediate dilution levels that the best efficiency is observed. This is interesting, considering the fact that columnar grains should have been the best suited for the transport of photogenerated carriers, as they can travel in the grains without the grain boundaries obstructing transport. However, experiments show that the samples grown at high dilutions do not show the best solar cell results. Meier et al. [94] observed that samples deposited at the highest dilutions ($SiH_4/H_2 = 1.25\%$) had high crystallinities and consisted of columnar grains up to 750 nm long. Such a structure is supposed to be most suitable for electronic transport in the perpendicular direction for a solar cell, since carriers will encounter a small number of grain boundary defects on their transport paths. However, such cells show the lowest open circuit voltage (V_{oc}). On the contrary, materials with small grains (at the transition between the crystalline and amorphous regimes), which would contain large grain boundary regions, show the maximum V_{oc}. However, there is one significant difference between the results of the Neuchatel and Julich groups. Whereas the former find structures with a (2 2 0) preferential orientation, the latter samples have randomly oriented grains.

In HWCVD deposition, the (2 2 0) oriented growth of μc-Si is more prominent at low hydrogen dilutions, which may be the key to good solar cell performance [73]. At high dilutions, the crystallographic orientation is more random. The importance of

(2 2 0) oriented growth for solar cell characteristics has been elucidated by many workers. Some of the best efficiencies, such as the results of the Neuchatel group [4] and Kaneka Co. [30], clearly point to this. Werner [95] has listed a number of results for laboratory cells which show high open circuit voltages, and this has been related to the (2 2 0) orientation of the poly Si. The importance of grain boundary activity for a (2 2 0) orientation is described in Section 5.1.3. However, one should be aware that microcrystalline films have an inhomogeneous growth pattern. This is manifested by a continuous change of structure in the initial stages of growth, before settling to a steady bulk structure. Kitagawa et al. [96] observed the change in order and disorder of the structure and the change in orientation during growth, using in situ RHEED, for their microcrystalline silicon samples made by conventional PECVD. The orientation along the (1 1 0) direction is initiated by a randomly oriented growth followed by a selective growth, and it is proposed that tilted (1 1 1) crystallites nucleate the (2 2 0) growth. A proper choice of seed layer can lead to device quality (2 2 0) oriented growth [70].

4.3. Impurities

The grain boundaries, which form major defect sites in poly Si material, can adversely affect the solar cell performance by impeding the flow of the majority carriers (which increase the series resistance) and by providing shunt paths in the poly Si layer (which reduce the V_{oc} and fill factor (FF)). The db defects at the grain boundaries can be passivated by hydrogen. A systematic improvement in polycrystalline cell I–V characteristics with hydrogen passivation has been demonstrated [97]. The second adverse effect of the grain boundaries is the effect of impurities located there. Incorporation during growth or segregation of oxygen to the grain boundary regions due to thermal annealing creates donor states. Kazmerski et al. [98] show that such states can be passivated by incorporation of hydrogen in these regions, where a chemical reaction between oxygen in the electronically activated grain boundaries and the hydrogen takes place. A similar behaviour is also observed in the passivation of acceptor states (B,Ga, In) in poly Si, which is dominated by Si–H interactions during hydrogen passivation [99].

For the case of microcrystalline silicon films, also grain boundaries are considered to provide shunt paths. AFM local current mapping of μc-Si films with oxygen impurities has shown that the conductivity at the grain boundaries is much higher than that inside the grains [55]. From the transport studies of HWCVD microcrystalline silicon films, Liu et al. [100] showed that oxygen contamination contributes 0.15 eV to the activation energy.

Torres et al. [101] showed that the n-type behaviour of μc-Si is linked to the oxygen content in the film and is an extrinsic effect which is not due to native structural defects. To avoid such donors, oxygen reduction by controlling the out-gassing of the reactor and purifying the feed gas are needed. For example, for a system with a low out-gassing rate of 1.1×10^{-6} mbar l/s, simply using a purifier reduces the oxygen content from 2.2×10^{22} to 2.5×10^{18} at/cm^3, with a corresponding reduction of the dark conductivity by more than three orders of magnitude.

However, the purifier is of little or no help if the out-gassing rate is not low enough. The effect of the purifier and donor reduction is clearly visible in the spectral response of a microcrystalline cell in the long wavelength region. It must be pointed out that before such an oxygen control procedure, the Neuchatel group had used a technique called microdoping [102] to compensate the donor states by incorporated boron. In fact, their first successful cell was fabricated by these intrinsic (low dark conductivity) i-layers made by microdoping to give an efficiency of 4.6% [3]. However, comparing the two procedures, oxygen reduction is a superior technique (comparing the cell efficiencies). It also should be noted that the oxygen intake of the film has a linear inverse correlation to the deposition rate [103]. Komoda et al. [53] found that poly Si films of high crystallinity suffer seriously from post-deposition oxidation, with the oxygen content reaching up to $5 \times 10^{21}\,\mathrm{cm}^{-3}$.

Kamei et al. [104] found no effect on grain size or crystalline volume fraction, as long as the oxygen incorporation is lower than $10^{20}\,\mathrm{cm}^{-3}$. Komoda et al. [53] proposed that oxidation occurs by breaking the Si–Si back bonds of SiH_2 complexes, with atomic oxygen inserted to bridge the Si atoms, forming Si–O–Si. It is inferred [104] that the oxygen impurities segregate at the grain boundaries and act as donors. The disorder of the grain boundaries and amorphous domains allows oxygen to fit readily into the structure, lowering the total energy of the system. A systematic increase of the carrier density with oxygen content (above $10^{18}\,\mathrm{cm}^{-3}$) is observed, given by the relation $n_e \propto [O]^{1.4}$. Such oxygen donors in microcrystalline silicon are considered as similar to thermal donor (TD) states in Czochralski Si, formed when the material is annealed at 400–500°C. It is proposed that in μc-Si material, oxygen incorporation is mediated by surface diffusion and this, being a thermally activated process, will allow the creation of films with less donors at lower growth temperatures. One of the unexplained results [104] is that for μc-Si samples made by VHF PECVD at a low T_s of 200°C, the ESR (neutral) defect density of $5–9 \times 10^{15}\,\mathrm{cm}^{-3}$ remains almost independent of oxygen concentration, as are the mobility and activation energy of 52–58 meV.

Depending on the local concentration of the oxygen-related shallow donors versus deep db defects; the donor electrons are expected to completely or partially compensate the deep defects, thereby reducing the spin density in microcrystalline silicon. This has a consequence in measurements of the defect density by ESR, where the intensity of neutral defects at $g = 2.0055$ underestimates the total number of defects. Upon illumination, this compensation is reversed by optical excitation of electrons from negative dbs (making them neutral) into shallow traps. This is manifested by an increase of the $g = 2.0055$ and $g = 1.998$ lines, both in LESR and SDPC measurements [88].

If oxygen incorporation degrades the material properties by creating donor states, hydrogen has the opposite effect. Its incorporation both during and after deposition has the ability to either inhibit the formation of donor states or compensate the effect. For VHF-CVD deposited microcrystalline silicon, Vetterl et al. [105] did not find any reduction in the dark conductivity as a consequence of boron microdoping (10^{18}–$10^{20}\,\mathrm{cm}^{-3}$), nor by reduction of the oxygen content in the film from 10^{19} to $10^{18}\,\mathrm{cm}^{-3}$. From this, they concluded that the films were truly intrinsic. This was

attributed to good hydrogen passivation of defects. Saito et al. [106] observed an increase in the resistivity of undoped polycrystalline silicon films during hydrogen passivation treatments. This was attributed to hydrogenation-induced passivation of the grain boundaries. Nasuno et al. [107] presented a model for the effective passivation of oxygen-related donors (which they presumed to be three fold coordinated oxygen) by hydrogen. The proposed mechanism was the insertion of hydrogen into Si–O bonds, i.e. $O{\equiv}Si + H \rightarrow H\text{–}Si + Si\text{–}O\text{–}Si$ where Si–O–Si is no longer electrically active. However, they contended that the mechanism of stability of the Si–H bond in the vicinity of the Si–O–Si bond is not yet clear. The high hydrogen content of 11% for the microcrystalline layers ((1 1 0) oriented) was considered to be the reason for the good passivation during deposition. However, the low surface diffusion rate of oxygen at low substrate temperatures may also make a contribution to a lower donor concentration. A high V_{oc} (which is controlled by the leakage current due to donors) was obtained in a solar cell, despite the presence of $2 \times 10^{19}\,cm^{-3}$ of oxygen in a μc-Si film grown at 140°C [107].

A reduction of the oxygen incorporation during growth can also be achieved by the choice of precursor gas. The use of a chlorinated precursor gas such as SiH_2Cl_2 has shown the possibility of depositing a microcrystalline sample at a much lower hydrogen dilution, and of yielding an easier nucleation process. However, such precursors have a more important positive effect in reducing oxygen incorporation in as-deposited samples. Intrinsic microcrystalline films have been fabricated by the PECVD process from $SiH_4/SiH_2Cl_2/H_2$, and the deposition process is very tolerant to changes in reactor conditions [108]. Microcrystalline films made from $SiH_4 + H_2$ showed a high electrical conductivity ($> 10^{-3}\,\Omega^{-1}\,cm^{-1}$) and a low activation energy ($< 0.2\,eV$), indicative of heavy doping with oxygen. Adding a few percent of SiH_2Cl_2 reduced the dark conductivity by five orders of magnitude, to $\sim 10^{-8}\,\Omega^{-1}\,cm^{-1}$, and an activation energy of $\sim 0.6\,eV$ was obtained. However, it is not clear whether oxygen reduction by a factor of two, by the use of chlorinated gas, can account for the five orders of magnitude drop in the dark conductivity (or films becoming more intrinsic), suggesting that other mechanisms may also be involved. Deactivation of O as a dopant by the presence of Cl is considered as a highly possible reason. The number of donors induced by the presence of oxygen can be reduced if the Si–O or Si–O–H bonds are replaced by much stronger Si–O–Cl bonds.

A number of observations have been made connecting the deposition parameters with oxygen and carbon incorporation. Konagai et al. [55] detected a high concentration of oxygen and carbon atoms in their HWCVD films. The oxygen content was of the order of 10^{20}–$10^{21}\,cm^{-3}$. Some of this comes from the chamber walls during deposition, and some are absorbed by the film from air after deposition. However, the oxygen depth profile in a poly Si/a-Si/poly Si multilayer system suggests that oxygen incorporation mainly depends on the pressure, and that the incorporation is predominantly during deposition. Matsumura [109] showed that although it is easy to make poly Si films by HWCVD at high pressure, it is the films made at low pressure (~ 1 mTorr), which show negligible contamination. In a narrow growth regime, it is also possible to obtain poly Si films with no oxygen contamination, and they are likely to show mobilities of several tens of $cm^2/V\,s$. A

relation between the SiH_4 gas flow rate, the gas pressure, the crystallinity and oxygen contamination has been observed [109]. Bruhne et al. [57] showed that for microcrystalline silicon films deposited by MVSystem filaments, there was no oxygen intake, and no change in the dark conductivity upon exposure to air or storage. On the other hand, films made using a Ta wire under the same conditions featured a large oxygen content. However, a high carbon content of 1% has been observed (for MV system filament grown films), and this has not yet been explained. Schubert et al. [110] studied the effect of impurities on the properties of HWCVD μc-Si material. They observed (by SIMS) a high concentration of carbon (2%) and oxygen (15% for the high vacuum system and 6% for the ultra high vacuum system) in the films. This result clearly shows the importance of the base pressure in relation to oxygen incorporation during deposition. On the other hand, VHF PECVD μc-Si films prepared in the same UHV deposition system contained only 0.2% oxygen. The sub band-gap absorption (defect density from PDS) showed a clear correlation with the oxygen content in the films (N_d(VHF PECVD) < N_d(HWCVD UHV) < N_d(HWCVD HV)).

Rath et al. [111] showed that oxygen incorporation in poly Si occurs in two ways: (i) in situ during growth and (ii) post-deposition. Two possible reasons are speculated for the oxygen incorporation; (1) the deposition rate and (2) the structure. The porosity and the hydrogen bonding configuration are identified as major causes of these processes. A high deposition rate, a compact structure and hydrogen at compact sites act as deterrents to oxygen incorporation in device quality poly Si made by HWCVD. It was proposed that high amount of oxygen penetration in poly Si films made at high hydrogen dilutions (Poly1) occurs by two processes: (i) oxygen incorporation during growth, and (ii) post-deposition oxygen intrusion. The first of these occurs due to a low deposition rate and the growth process. The second is due to the intrusion of water vapour into the film through the voids, which increases the electrical conductivity in proportion to the amount of intrusion. It was shown that their device quality compact poly Si:H (Poly2—made at a low hydrogen dilution) resists oxygen incorporation even when deposited in an oxygen-rich atmosphere. This was confirmed by oxygen depth profiling of HWCVD poly Si films. SIMS analysis showed that the oxygen concentration in the bulk of a Poly2 specimen is $3 \times 10^{18}\,cm^{-3}$, and the oxygen content drops to this value only 50 nm from the surface. The IR spectrum of Poly1 material (Fig. 5) shows a strong Si–O_x band ($\sim 1050\,cm^{-1}$), which is absent in Poly2 films. The IR spectrum of Poly2 films deposited even with a deliberate leak in the chamber (low base pressure) showed no oxygen-related absorption, even under these leak conditions. For a *profiled* film (Poly2 on Poly1) it was also the case that no Si–O_x IR absorption could be seen. Electronic transport studies also showed the effect of oxygen on HWCVD Si films. During heating, the oxygen or water vapour, which is presumably incorporated, diffuses out from the Poly1, and the electrical conductivity during the cooling cycle is lower than that during the period of ramping up the temperature. For the conductivity of Poly2 measured at a similar time after the deposition, the heating and cooling cycles coincide. A single activation energy of 0.54 eV is obtained for the dark conductivity for this film, with a band gap of 1.1 eV. This confirms that the Fermi

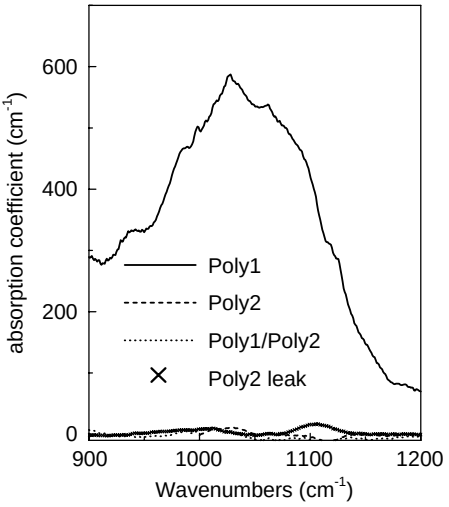

Fig. 5. FTIR spectra of poly Si films made by HWCVD at Utrecht University [111]; Poly1: high hydrogen dilution, Poly2: low hydrogen dilution, Poly1/Poly2: double layer called a *Profiled layer*. The Poly2 leak sample ($\sim$1500 nm) is Poly2 made with an air leak in the deposition chamber.

level is exactly at the centre of the gap, and that the material is truly intrinsic. For the case of a so-called profiled layer where Poly2 is deposited on top of Poly1, little variation in conductivity is observed as a consequence of annealing. This suggests that Poly2 acts as a good capping layer to prevent oxygen diffusion.

4.4. Optical properties

An enhanced optical absorption has been observed in microcrystalline silicon films. Meier et al. [3] showed that, though a microcrystalline silicon film has the same optical gap as c-Si, the absorption coefficient is almost an order of magnitude higher. Thus, only a $\sim$2 μm thick layer is necessary for the microcrystalline cell compared to the $>$100 μm thick wafer used for a c-Si cell. The enhanced light absorption in these microcrystalline films and solar cells has been attributed mainly to the longer optical path which occurs as a result of efficient diffused light scattering at the textured film surface. The optical properties (absorption coefficient) of microcrystalline silicon films have been modelled using the effective medium approximation. They are modelled either as a two-phase system of a-Si and c-Si [112] or a three-phase system of a-Si, c-Si and grain boundaries [113]. Diehl et al. showed [113] that elastic light scattering is not mainly responsible for the enhanced absorption, especially in the range 1.4–2 eV. The absorption in this region is a superposition of the absorption coefficients of the crystalline grains, the grain boundary regions and the amorphous phase weighted by the corresponding volume fractions. The grain boundary absorption is enhanced due to relaxation of the k-selection rule, and is also influenced by the hydrogen content at the grain boundaries.

Three distinct regions of the absorption spectra have been explored [114]: (i) the region between 1.2 and 1.4 eV, (ii) absorption above 1.5 eV and (iii) the sub-gap region below 1.1 eV. It has been shown [114] that absorption below 1.4 eV is predominantly due to surface scattering (due to surface texture) and, in the case of porous materials, a contribution from bulk scattering at the voids is also present. However, by polishing the material or using scattering modelling, the true optical absorption can be obtained. This is the same for microcrystalline silicon as for c-Si, being between 1.2 and 1.4 eV. The absorption above 1.5 eV has mainly been attributed to the amorphous component, though other contributions are also speculated. The sub-bandgap absorption is correlated to the defect absorption. Here, it should be emphasised that the indirect band gap of microcrystalline silicon is 1.1 eV. The band gap is estimated from a plot of $\sqrt{\alpha}$ versus $h\nu$ (where α is the optical absorption coefficient and $h\nu$ is the energy). The absorption spectra for this are obtained by PDS or CPM in the low-energy region, in contrast to the case of amorphous silicon where (due to high absorption and the high optical gap) the absorption coefficient measured by simple reflection/transmission gives the optical gap either as Tauc's gap (obtained from a $(\alpha h\nu)^{1/2}$ versus $h\nu$ plot) or a cubic gap (represented by a $(\alpha h\nu)^{1/3}$ versus $h\nu$ plot). There are a few differences between amorphous and microcrystalline silicon, in respect of the absorption spectra and the parameters that are derived from them. The Urbach energy, E_0, defined from the relation $\alpha = \alpha_0 \exp(E/E_0)$ and obtained from the exponential region of the optical absorption spectrum, is manifested as a linear region in the $\log \alpha$ versus $h\nu$ plot. For microcrystalline silicon, this inverse slope is not always clearly visible. Vanecek et al. [114] observed such a linear region, attributed to the Urbach tail, and correlated it to the valence band tail width. This is between 50 and 60 meV. Significantly, this value is very similar to the E_0 of $\sim$50 meV obtained for amorphous silicon.

Van Veenendaal et al. [115] reported that their polycrystalline silicon films made by HWCVD also showed an enhanced optical absorption coefficient compared to c-Si. However, their interpretation was quite different [114]. From various experiments (atomic force microscopy, angular resolved light scattering, photothermal deflection spectroscopy, reflection/transmission, Raman spectroscopy), performed on as-deposited and polished layers, it was concluded that the main contribution to the enhanced absorption in their HWCVD poly Si:H films was not due to the presence of an amorphous phase, nor to surface scattering, but rather due to a strained layer near the initial deposition region. The results of angular resolved light scattering measurements performed on as-deposited and polished poly Si films showed that the former have a significant diffuse reflection, which correlates to the surface texture of the poly Si. Polishing the film reduces the diffuse reflection, as a result of a decreasing surface roughness. However, it does not change the optical absorption coefficient. This indicates that the influence of surface scattering upon the enhanced absorption is only minor. The overall absorption coefficient gradually decreases with increasing thickness, due to the reduced contribution of the strained layer to the total thickness of the film. The presence of the strained layer was confirmed by the Raman spectrum, measured from the back side (through the glass substrate). This was also

confirmed in simulation studies of solar cell devices [113]. However, from the angular resolved light scattering measurements, it follows that surface scattering has a negative effect; namely optical loss due to diffuse reflection. In a solar cell, this loss is reduced by the presence of a TCO coating.

4.5. Electronic transport

Carrier transport in a multiphase system such as microcrystalline/polycrystalline silicon is complex. Moreover, grains of various dimensions and orientations make the transport path even more complex. However, some distinct features of the electronic transport in these films, and their relevance to device performance, have been reported by several workers. The inhomogeneity of the microcrystalline structure (for example for a μc-Si sample made with 5% silane in hydrogen dilution by VHF-PECVD at IMT, Neuchatel) is best illustrated by the range of activation energies estimated by different measurement methods: 0.14 eV for the electron drift mobility (TOF measurement), 0.29 eV for the AC conductivity, 0.4 eV for the steady-state dark conductivity and $\geqslant 0.8$ eV for the photocapacitance relaxation [117]. As will be shown below, there are three special characteristics of μc-Si concerning its transport properties: (i) the energy barrier between grains, (ii) the anisotropy of the electronic transport, (iii) the thickness dependence of the electronic properties.

Electronic transport studies in a planar configuration (though not very relevant to solar cell operation where carrier transport is in the perpendicular direction) gives valuable information about the trap density at the grain boundaries. Kudrna et al. [118] studied the carrier diffusion by a picosecond laser grating technique in a microcrystalline film with a complicated microstructure containing both large and small grain boundaries (samples from IMT, Neuchatel). Sometimes, the large grains constituted small crystallites (spherical or columnar) and it was investigated whether the diffusion coefficient of the carriers was limited by the boundaries of the small grains. They obtained a diffusion coefficient, D, of 9 cm^2/s for a sample grown using a 1.25% silane in hydrogen. This is slightly smaller than, but comparable to, that for bulk c-Si (10–16 cm^2/s). Considering the fact that the above films constitute crystal columns (perpendicular to the substrate) of 750 nm average length and 24 nm diameter, the high diffusion coefficient (measured perpendicular to the grain boundaries) implies that small grain boundaries do not form potential barriers. This supports the idea that they preserve a tetrahedral coordination (such as tilted grain boundaries) and the lack of carriers prevents the formation of depleted regions. This allows for an easy carrier passage. In fact, the estimated diffusion length is 1 μm (from $L^2 = D\tau$), which is much larger than the grain dimension along the transport path (24 nm). However, the barrier at the grain boundary very much depends on the structure. For example, for the case of poly Si films (made at UU by HWCVD) with large grains (average grain size ~ 70 nm), a very small activation energy (0.012 eV) of the Hall mobility was obtained [51]. This shows a very small barrier to transport at the grain boundaries, which is attributed to a [110] tilted type grain boundary in a (2 2 0) oriented growth.

The anisotropy of the electronic transport in microcrystalline silicon is caused by the orientation of the grains and the location of grain boundaries with respect to the transport path. This has significance when one tries to correlate the material properties to the device performance. To be more specific, transport studies in a perpendicular direction are more relevant to the solar cell performance, whereas transport in a planar configuration can be correlated to the performance of thin film transistors made with a μc-Si active layer. Kocka et al. [119] have shown that the complex AC conductivity can be used to measure the conductivity in the perpendicular ($\sigma_\perp$) direction (by measuring the conductivity of a microcrystalline sample in a sandwich configuration), where the effects of contacts can be minimised. The empirical rule for the determination of $\sigma_\perp$ is to find a "plateau" in the conductivity at frequencies large enough for the exclusion of the impedance of the depleted regions. In some samples, two sets of plateaus appear, which indicates that the $\sigma_\perp$ changes with thickness. A comparison of $\sigma_\perp$ with the conductivity parallel to the substrate, $\sigma_\parallel$ (measured by DC conductivity in a planar configuration), showed an anisotropy in the electrical transport properties. This was again confirmed by a comparison of the carrier diffusion lengths measured in the parallel configuration, $L_\parallel$ (measured by the steady-state photo carrier grating (SSPG) technique) and the perpendicular configuration, $L_\perp$ (measured by the surface photo voltage, SPV) [120]. Both $L_\parallel$ and $L_\perp$ increase with increasing thickness. However, at all thicknesses, $L_\perp$ is several times higher than $L_\parallel$. Extending this work to a supperlattice containing alternate amorphous and microcrystalline sub-layers, it was observed [119] that in such a structure the transport is isotropic ($\sigma_\perp = \sigma_\parallel$ and $L_\perp = L_\parallel$). What is interesting is that in a superlattice (containing small grains) with a 76% μc-Si:H fraction, $L_\perp = L_\parallel = 300\,\text{nm}$. However, in a purely microcrystalline structure (100% μc-Si:H fraction) $L_\perp$ is the same as for the superlattice (300 nm), whereas $L_\parallel$ is much smaller due to the presence of crystal columns. Kocka et al. [121] argued that in a microcrystalline silicon film where $\sigma_\perp \gg \sigma_\parallel$, (as a result of a high $\sigma_\perp$ due to the columnar structure), this may cause shunt leakage through grain boundaries and decrease the open circuit voltage. It has been proposed that the isotropic conductivity is the key to a high V_{oc} and efficiency, and that from this point of view a superlattice is a good candidate. This claim is supported by measurements on a μc-Si sample from ETL, which gave a 9.4% efficiency in solar cells. These materials made at 150°C show isotropic transport properties ($\sigma_\perp \approx \sigma_\parallel \approx 10^{-6}\,\Omega^{-1}\,\text{cm}^{-1}$ and $L_\perp \approx L_\parallel \approx 300\,\text{nm}$). This result would suggest that anisotropic columns may be unnecessary for achieving photovoltaic conversion in μc-Si:H based solar cells.

An anisotropy of the carrier transport in (2 2 0) preferentially oriented polycrystalline silicon films fabricated by VHF CVD with SiF_4/H_2 gas has been observed by Nakahata et al. [122]. They observed that for samples made at $T_s = 150°C$, the $\sigma_\perp$ (AC conductivity in a sandwich structure) and $\sigma_\parallel$ (DC conductivity in a planar configuration) are similar. However, for samples made at $T_s = 200$ and 250°C, $\sigma_\perp$ is five times or ten times (respectively) larger than $\sigma_\parallel$. However, the activation energies of $\sigma_\perp$ and $\sigma_\parallel$ are similar for both deposition temperatures (0.47–0.49 eV). This correlates with the increased crystallite size perpendicular to the substrate and with the decrease of orientation fluctuation with increasing substrate temperature,

although all the samples have (2 2 0) oriented grains and the crystalline volume fraction is similar (80–90%).

Unlike amorphous silicon, microcrystalline silicon shows an inhomogeneity in its electronic properties. The depth dependence of the electronic transport in microcrystalline silicon films has been reported by various researchers. Studying the dynamics of photogenerated carriers by using optically pumped terahertz probe measurement, Jepsen et al. [123] observed that microcrystalline films (in this case ECR CVD samples from HMI, Berlin) showed depth-dependent electronic properties, which manifest themselves in the THz transient (from 400 and 800 nm excitations). The transients have two components: a fast initial decay due to carrier capture in trapping states, followed by a slow decay due to carrier recombination.

Using real time microwave mobility measurements, Brenot et al. [124] showed that there is an increase in the average carrier mobility as a function of film thickness, which is compared with the increase of the crystalline volume fraction. Such an experiment combines time resolved microwave conductivity (TRMC), which gives the product of the microwave mobility and the excess free carrier concentration generated by the laser pulse, and spectroscopic ellipsometry (SE), which gives the concentration of photogenerated carriers. The significant observation is that the saturation of the crystalline volume fraction above 200 nm thickness does not lead to a saturation in the effective mobility (sum of electron and hole mobilities). The authors proposed that the electron drift mobility is not only a function of crystalline fraction, but is also influenced by the defect density, grain size and quality of grain boundaries. A similar observation was made by Kocka et al. [119], where an improvement in the transport properties (conductivity and diffusion length) with thickness has been correlated with different grain sizes, whereas the crystallinity (crystalline volume fraction) of films thicker than 1 μm is nearly the same. From the combination of TRMC and ellipsometry measurements, Brenot et al. [125] showed that transport is not controlled by the amorphous tissue between crystallites. However, the amorphous phase at the substrate interface can degrade the transverse transport properties. With a better quality of crystallites, electron and hole mobilities larger than $10\,cm^2/V\,s$ can be achieved. From this, these authors concluded that transport in microcrystalline silicon is controlled by defects inside the crystallites, and not by barriers between them.

Van Veenendaal et al. [126] studied the time resolved microwave conductivity of poly Si films made by HWCVD. By using short wavelength light (320 nm) for excitation, the mobilities at the top surface and near the substrate interface were compared for three types of sample. For Poly1 (a sample made at high hydrogen dilution), the mobility is similar ($\sim 1\,cm^2/V\,s$) for both cases, but carriers have a very low lifetime (less than 1 ns). This is consistent with homogeneous and highly microcrystalline growth (without incubation) combined with highly defective ($N_d \sim 10^{18}/cm^3$) grain boundaries and small grains. For a Poly2 (lower dilution) sample, the mobility at the substrate interface is 20 times smaller than at the top ($\sim 4\,cm^2/V\,s$), confirming the amorphous incubation. In the case of a profiled layer (Poly2 on top of a Poly1 seed layer), the mobility at the substrate interface is

somewhat improved. More important is the improvement in the lifetime of the Poly1 seed layer in the profiled layer structure, compared to the individual Poly1 layer. This suggests a modification of the grain boundary properties of the seed layer, which may have a positive effect on the solar cell properties (a profiled layer is used in solar cells at UU [52]). The experiment shows that it is possible to probe the mobilities and lifetimes of charge carriers in different parts of a thin polycrystalline silicon layer by using TRMC. In this particular case, it was shown that profiled growth conditions for poly Si films enhance the mobility in the substrate region, while leaving the high mobility in the top region largely unaffected.

5. Solar cells

5.1. Single junction

In this section, in addition to the efficiencies of single junction microcrystalline solar cells, the importance of the substrate and its development along with sophisticated back reflectors will be discussed. At present, two types of solar cell configurations are followed: (i) The superstrate type, where p, i and n layers are deposited in this sequence on top of the substrate and light enters through the substrate and (ii) the substrate type, where n, i and p layers are deposited in this sequence on the substrate and light enters through the top. The choice of configuration is decided by the type of substrate, and vice versa. The processing temperature also plays an important role in deciding the type of substrate and configuration.

5.1.1. Substrate

For the efficient use of a microcrystalline silicon solar cell, two aspects are pursued: a high deposition rate, which will allow for a high throughput, and highly efficient light trapping which will allow a reduction of the cell thickness. For the latter, the back reflector and the substrate technology are very important.

The structure of a poly Si in a solar cell can be very much different from the test material made on a glass substrate. This is mainly due to the texture of a TCO for p–i–n cell or any back reflector in an n–i–p cell. Meier et al. [127] looked at the structure of a microcrystalline silicon cell on a ZnO substrate. Close to the ZnO, crystals which are several tens of nanometers long grow perpendicular to the ZnO facets. Further away, the crystals grow perpendicular to the average substrate plane and the crystal column lengths reach several micrometers. Aggregates of small crystallites (of a few tens of nanometer diameter) constitute every column of several hundreds of nanometers, which is loosely packed at the substrate interface and dense towards the top. A surprising observation is that a cell which shows a high V_{oc} exhibits voids at the ZnO p/i interface. The Julich group [128] observed that columnar growth always occurs perpendicular to the substrate surface, and for a textured surface such a growth results in a fan-like arrangement at the cusp of the

TCO surface. Because of the shadowing effect, large voids are formed within grooves, which extend throughout the layer. However, this group has not yet seen any detrimental effect of this texture upon the solar cell performance. On the other hand, a definite correlation between the defects caused due to columnar growth on a textured surface with solar cell performance has been observed by Nasuno et al. [129]. A correlation between the surface morphology and the solar cell characteristics has been established. Two types of surface: glass/ZnO and glass/SnO_2 coated with 500 nm ZnO, texturised with wet etching with 0.5% HCl, were investigated. A parameter which has been introduced is the average slope of the surface texture, given by $\theta = (2 \times \mathrm{RMS})/(\lambda/2)$ where RMS is root-mean-square height measured by AFM, and λ is the average width of the surface roughness modulation measured from the peak position in the powder density spectrum obtained by Fourier analysis of the AFM images. Columnar growth is limited by the collision of columns, which are perpendicular to the local surface of the textured substrate. Nasuno et al. [129] proposed that this would lead to grain boundaries and would result in a systematic reduction of V_{oc} and FF with increasing $\tan\theta$, attributed to carrier recombination at the grain boundaries. Hence, a compromise between light trapping (increase of J_{sc} with $\tan\theta$ up to saturation) and grain boundary formation is needed, which gives the optimum value of $\tan\theta = 0.08$. On a smooth surface, the collision does not occur, which leads to a reduced number of grain boundary defects.

The quality of growth of the doped μc-layers on the TCO layer is important, not only for the barrier at the TCO/doped layer interface but also for the quality of the intrinsic layer on top of the doped layer, which may act as seed layer. While looking at the ZnO/p-μc-Si interface, Vallat-Sauvain et al. [130] found that the X-ray diffraction spot of the ZnO crystal lies on the (2 2 0) silicon diffraction ring, and they obtained a similar d-spacing of the ZnO(1 0 2) planes and the Si(2 2 0) planes. This is correlated to the $d_{Si220} = 0.19201$ nm and $d_{Zn102} = 0.1911$ values from literature. The small heterogeneity $\Delta d/d$ of only 0.47% leads to a good electrical contact between Si layers and the ZnO. This lattice matching results in p-layer growth without any incubation phase. It is claimed that this has a significant effect on the performance of microcrystalline solar cells. Ahn et al. [131] proposed that films such as calcium (CaF_2), strontium (SrF_2) and barium (BaF_2) fluoride are good seed materials for μc-Si growth, because they have the same cubic structure as c-Si and similar lattice constants. The μc-Si films were deposited on CaF_2/glass substrates by remote plasma CVD. The grain size can be doubled for μc-Si on a CaF_2/glass substrate in comparison to μc-Si on SiO/glass. It is proposed that (1 1 1) preferred CaF_2 films are useful for device applications, because they exhibit the lowest lattice mismatch with Si (68%), and this is beneficial because CaF_2 films have a (1 1 1) preferential orientation, which requires less energy.

One of the most important criteria for the choice of TCO for microcrystalline cells is its ability to withstand the large atomic hydrogen flux reaching the TCO surface during the growth of the microcrystalline layers. SnO_2 is significantly reduced in a hydrogen plasma. ZnO has proved to be important for the microcrystalline cells because of its better resistance to a hydrogen plasma. Meier et al. [127] claimed that LP-CVD ZnO exhibits a superior performance compared to SnO_2 (U-type). ZnO

coated textured SnO_2 substrates are also used to protect the SnO_2. However, the barrier at the ZnO/p interface is very critical. Yamamoto et al. [132] showed that by using a thin non-hydrogenated amorphous silicon layer (formed by magnetron sputtering in an Ar Plasma, hydrogen 1%, defect density $1.5 \times 10^{19}\,cm^{-3}$) at the SnO_2/p interface, the p-layer quality is as good as on a ZnO coated SnO_2 surface and the darkening effect is completely removed (as well as for ZnO coated SnO_2). However, no crystallinity can be observed on a virgin SnO_2 surface, and the darkening effect is completely removed (as well as for ZnO coated SnO_2). This layer also removes the barrier at the TCO/p interface, and provides a lot of trapping sites for the hydrogen from the p-layer during deposition. Moreover, a disordered a-Si layer surface is good for nucleation of the microcrystalline p-layer [133]. An improved open circuit voltage and current leads to a better efficiency compared to SnO_2, ZnO/SnO_2, or ZnO substrates.

5.1.2. Solar cell performance

In this section, the performance of solar cells with an i-layer deposited by various PECVD and other techniques is presented. In all cases, the efficiency of the cells should be evaluated with respect to the process temperature and growth rate.

RF PECVD: Though VHF PECVD has been shown to be very suitable for device quality poly Si for solar cells, at high frequencies scaling up from $1\,cm^2$ to large panels is difficult. Because of industrial scale-up simplicity, attempts have been made to produce poly Si solar cells by standard frequency (13.56 MHz) PECVD at high deposition rates.

Yamamoto et al. [30] obtained an efficiency of 10.7% (aperture area efficiency of 10.1%) for an n–i–p cell in a configuration called a second-generation "STAR" (naturally Surface Texture and enhanced Absorption with back Reflector) structure. The first generation poly Si STAR cells were in the configuration glass/back reflector/n-layer/i-poly Si/p-layer/surface texture/ITO/Ag gridline, whereas the second-generation cells employed texture at the back reflector. The i-layer (grown at $\sim 550^{\circ}C$) was deposited by RF PECVD. Though the i-layer was meant to be intrinsic (without intentional doping), actually it was slightly n-type (phosphorus content of $5 \times 10^{15}\,at/cm^3$) and the incorporation of oxygen impurities was also assumed. The parameters of the cells were $V_{oc} = 0.539\,V$ and $J_{sc} = 25.8\,mA/cm^2$ for an i-layer thickness of $2\,\mu m$. A quantum efficiency (QE) of 60% at 800 nm explains the beneficial effect of good light trapping. It was shown that the carrier concentration and thickness of the i-layer sensitively affects the V_{oc}, and that a higher V_{oc} is achieved with a higher carrier concentration (achieved by phosphorus in the i-layer). In a later development [134], Kaneka Co. has tried a p–i–n superstrate configuration, for which a low temperature approach was used. However, the performance of an n–i–p poly Si cell is better in single-junction cells, because of the wider process windows for forming both back reflectors and each layer of the Si film.

Rech et al. [135], following the model suggested by ETL group (HPD method), have been able to make device quality poly Si films at high deposition rates using high pressures and powers. Cells were made in a superstrate configuration on texture-etched ZnO coated glass substrates, and with a ZnO/Ag back reflector in the

configuration glass/ZnO/p-μc-Si/i-μc-Si/n-a-Si:H/metal. The FF and V_{oc} were monitored for optimisation. All the μc-Si films were made close to or in the regime of silane depletion. The transition between the amorphous and crystalline regimes in the solar cell configuration was deduced from the observation that a significant response in the infrared region is indicative of a crystalline region, and a low infrared response combined with a high V_{oc} (>600mV) indicates amorphous material. In the optimisation process, it is manifested as a sudden drop in the short circuit current density (losses above 600 nm are due to a reduced crystalline fraction and losses below 600 nm are due to a carrier collection problem) at the transition. Efficiencies of 8.1% (films made at 10 Torr and 0.5 W/cm^2, $SiH_4/H_2 = 0.8\%$, i-layer = 1.2 μm) and 7.5% for deposition rates of 0.5 and 0.9 nm/s, respectively (for p–i–n cells made at temperatures $\leqslant 200^\circ$C) have been achieved. This group also achieved 6.6% for films made at 1.0 nm/s. The success is attributed to the "soft" deposition parameters (low ion energy) for achieving high-pressure deposition while maintaining a high deposition rate by high power. However, one of the observations to be remembered in the scaling up process is the rather small window of parameter space for the best efficiency. P–i–n microcrystalline solar cells on 30×30 cm^2 substrates showed an efficiency of 8.1% (FF = 0.724, $V_{oc} = 0.555$ V, $J_{sc} = 20.2$ mA/cm^2) at a deposition rate of 0.5 nm/s. Rech et al. [136] concluded that a substrate temperature above 200°C in a p–i–n configuration should be avoided, due to the heat sensitive p/i interface.

Using standard RF PECVD, Nasuno et al. [137] made an n–i–p solar cell in the configuration p-μc-Si/i-μc-Si/p-μc-Si/ZnO/Ag on Asahi SnO_2 and ZnO coated substrates, and attained efficiencies of 8.9% and 9.4% ($V_{oc} = 0.526$ V, FF = 0.71, $J_{sc} = 25.3$ mA/cm^2), respectively. The deposition rate was 0.15 nm/s at $T_s = 140^\circ$C, for films with a grain size of 18 nm. The efficiency decreased with increasing deposition rate, achieved by increasing power in the RF PECVD: the efficiencies were 7.5% and 4.6% at 40 W (0.5 nm/s) and 110 W (1.0 nm/s), respectively. However, they found that increasing the frequency was an efficient way to further increase the deposition rate without affecting the device quality. They could achieve an efficiency of 8.1% at 60 MHz, at a deposition rate of 1.2 nm/s and a temperature of 150°C.

VHF PECVD: Meier et al. [138] showed that as the properties of microcrystalline films on glass are different from those in the cell structure, analysis of the properties in the cell configuration and cell characteristics should be used to define the microcrystalline nature of the i-layer. This is particularly important, since the best poly Si cells seem to be made in the transition region from the amorphous to the crystalline state. Cells which show an enhanced infrared response at >750 nm are considered to be microcrystalline. The general trend is that V_{oc} increases with decreasing dilution. A high dilution sample has a high crystallinity and shows long columnar grains. Such a structure is best suited for electronic transport in the direction perpendicular to the substrate (where there are less grain boundaries to overcome). However, they lead to a smaller V_{oc}. Instead, films with smaller grains (at lower dilution) and higher numbers of grain boundaries give a better V_{oc}. A phenomenological explanation of this is given by Kocka et al. [121]. A V_{oc} as high

as 0.56–0.58 V has been achieved while maintaining a high FF. The best p–i–n cell (made at 200°C) efficiency, as obtained by the Neuchatel group using VHF PECVD is 8.5% ($V_{oc} = 0.531$ V, FF = 69.8 and $J_{sc} = 22.9\,mA/cm^2$). N–i–p Type cells [139] made on glass/Ag/ZnO and steel/Ag/ZnO substrates with an i-layer made using the same deposition process, showed an efficiency of 7.8% (2 μm i-layer, $J_{sc} = 24\,mA/cm^2$, $V_{oc} = 0.462$ V, FF = 0.7) at a deposition rate of 0.74 nm/s, and 6.9% (4 μm i-layer) at a deposition rate of 1.0 nm/s.

Using VHF PECVD at 95 MHz and $T_s = 200°C$, the Julich group [91] developed a p–i–n solar cell with an efficiency of 8.1% at a deposition rate of 0.15 nm/s. Verterl et al. [140] used the same method to make n–i–p cells on a ZnO substrates with efficiencies of 8.7% and 8.2% at deposition rates of 0.2 and 0.46 nm/s, respectively. As the deposition rate is limited by the substrate, it is interesting to see a clear observation in the case of n–i–p or p–i–n cells that a high deposition rate is correlated to a high process temperature (a linear relation is observed). For an n–i–p cell, a weak dependence of the solar cell efficiency on thickness from 1 to 3 μm was observed due to the combined changes of V_{oc}, FF (decrease) and J_{sc} (increase) with increasing thickness. Moreover, efficiency in n–i–p cells is improved at high deposition temperatures, with a peak at 250°C, whereas p–i–n cells show no such improvement. Rather, the degradation is more severe at temperatures higher than 250°C [137].

Suzuki et al. [34] described the performance of a solar cell in the configuration glass/Ag/ZnO/n-i(2 μm)-p/ITO/Ag. The μc-Si i-layer was deposited at a rate of 5.8 nm/s by VHF PECVD (60 MHz) in combination with a triode configuration and a showerhead cathode, using the HPD method from a SiH_4/H_2 mixture. For this cell, they reported an efficiency of 3.4% ($J_{sc} = 10.7\,mA/cm^2$, FF = 0.59 and $V_{oc} = 0.54$ V).

Saito et al. [141] from Canon Co. obtained an efficiency of 10.87% with an i-layer deposited at a rate of 0.4 nm/s by VHF. Other parameters were FF = 0.70, $V_{oc} = 0.518$ V and $J_{sc} = 29.96\,mA/cm^2$. The cell structure was SS/Ag/ZnO/n^+(20 nm)/i-μc-Si($\sim$2.28 μm)/p^+(5 nm)/ITO/grid. The gas residence time was used as the key parameter for cell optimisation. The best cell was obtained with a small residence time, which depends on combinations of the gas flow rate, pressure and plasma volume. This was attributed to a lower level of powder formation. The parameter space was $T_s = 100-400°C$, $P_r > 10$ Pa and power $> 0.1\,W/cm^2$. In the high deposition rate regime [142], they made a μc-Si solar cell with an efficiency of 5–6.5% deposited at a rate of 1.5 nm/s. Although the actual process steps for increasing the deposition rate were not specified, it is believed that the high growth rate was primarily achieved by a high power and pressure. The importance of a high gas flow rate for achieving good microcrystallinity has been demonstrated. This is manifested in a systematic increase in the crystalline volume fraction, a low defect density and a higher efficiency for a series of cells made at the same deposition rate of 1 nm/s. An efficiency of 9.56% for solar cells deposited at a rate of 1.2 nm/s on large area (35.6 cm × 700 cm) SS in a roll-to-roll process has been achieved by VHF-PECVD.

Matsui et al. [143] from Osaka University made an n–i–p solar cell in the configuration glass/SnO_2/Ag/ZnO/n(75 nm)-i(3 μm)-buffer/p (35 nm)/ITO/grid, with

an i-layer made by VHF PECVD (100 MHz) at a rate of 0.31 nm/s from SiH_4/H_2 at $T_s = 180^\circ C$. A glass/SnO_2/Ag/ZnO back reflector with surface roughness was used. Optimisation of the process parameters was monitored by the performance of the solar cells and the cell parameters. Large columnar grains (grain size 30 nm) were grown perpendicular, in the (2 2 0) preferential direction. The V_{oc} decreased monotonically with increasing crystalline volume fraction, whereas poly Si with $V_f >$ 50% and (2 2 0) preferential orientation is necessary for a high J_{sc}. The optimum cell performance was obtained at around V_f of 50%, where the V_{oc} and J_{sc} product was a maximum. A thin a-Si buffer layer at the p–i interface was shown to improve V_{oc} and FF. The maximum conversion efficiencies obtained were 7.91% with FF = 0.70, $V_{oc} = 0.507$ V and $J_{sc} = 22.3\,mA/cm^2$.

The VHF technique allows high quality of microcrystalline films to be made at low substrate temperatures, and the only report of a microcrystalline solar cell on a plastic substrate was for the one made by VHF CVD. Substrate type n–i–p cells have been fabricated on the polymer substrate E/DT (Ethylene-tetracyclododecene copolymer: heat deformation temperature 135°C, low water adsorption $<0.01\%$, water transmission 0.09 gm^2/mm day) [144]. The cell configuration was polymer/Ag/ZnO/n(50 nm)–i(1800 nm)–p(30 nm)/ITO/Ag, with an i-layer grown at 100°C. The efficiency was 6%. Texturisation of the polymer substrate was achieved by using a stamper on which a textured surface was replicated, and a RMS roughness of 30 nm was used.

Microwave PECVD: Jones et al. [145] reported on solar cells in an n–i–p structure using μc-Si made by a gas jet technique for the i-layer. They obtained a stabilised efficiency of 7% with white light and 2.7% with red light (>610 nm). The degradation with white light was 2–5%, after soaking for 1000 h. The authors agreed that the efficiency was lower than the highest one achieved in the world so far, but very comparable to the case of VHF μc-Si, where high deposition rates were tried.

HWCVD: Rath et al. [51] reported the first working solar cell (on n^+c-Si surface) incorporating a HWCVD grown poly Si i-layer, with 3.15% efficiency. This was followed by a real thin film solar cell on an SS substrate [52], made in the substrate configuration SS/n-μc-Si:H(PECVD)/i-poly Si:H(HWCVD)/p-μc-Si:H(PECVD)/ITO. A TEM image of the cross-section of the solar cell is shown in Fig. 6. The n-μc-Si:H and p-μc-Si:H films were made by PECVD at a substrate temperature of about 200°C, whereas the i-layer was deposited by HWCVD at $T_s = 500^\circ C$ in the same multichamber system. In order to improve the initial deposition of the poly Si:H layer and to make device-quality poly Si:H films avoiding any amorphous incubation phase, *profiled* poly Si:H layers were made by integrating two growth regimes: a Poly2 layer (low hydrogen dilution) was deposited on top of a Poly1 layer (high hydrogen dilution) of a certain thickness (see Fig. 2). The quality and growth of *profiled* poly Si films made with Poly1 seed layers of different thicknesses was monitored. The aim was to make the seed layer as thin as possible, in order to avoid the recombination of photogenerated carriers in this rather defective layer. At a Poly1 seed layer thickness of 20 nm, an optimum efficiency of 4.41% and a FF of 0.607 were achieved. A current density of 19.95 mA/cm^2 was generated with an i-layer only $\sim 1.22\,\mu m$ thick, that was deposited at a rate of more than 0.5 nm/s.

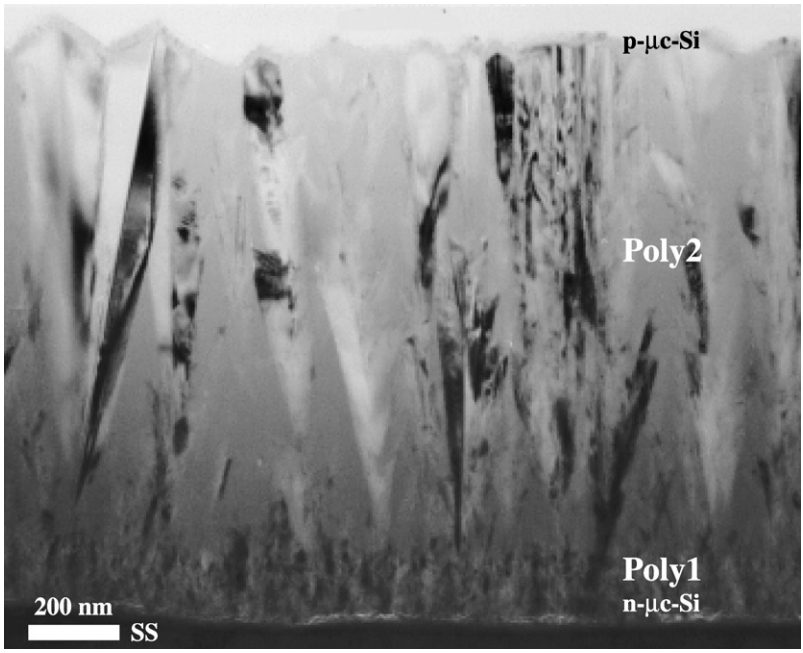

Fig. 6. Cross-section of a solar cell (SS/n–i–p/ITO/Ag) made at UU, as measured by XTEM [52].

Using a poly Si i-layer made by the variable dilution method based on the concept proposed by Rath et al. [73], a solar cell has been made (at Ecole Polytechnique, Paris) in the configuration glass/SnO_2/n–i(2.6 μm)–p/Ag (area 0.12 cm^2). This showed an efficiency of 4.6% [146]. The n and p microcrystalline layers were 50–60 nm thick, and were made by 13.56 MHz PECVD. The i-layer, deposited at 200°C, had a crystalline volume fraction of 60%. The other cell parameters were FF = 0.58, $V_{oc} = 0.40$ V and $J_{sc} = 19.8$ mA/cm^2. However, it should be noted that the light entry was from the n-side, which is the opposite to that for the expected structure in the case of amorphous silicon. The mobilities of electrons and holes, and their difference, play a crucial role in defining the structure of the cell for the collection of the carriers. Recent reports show that in case of PECVD μc-Si samples, the carrier collections by n–i–p and p–i–n structures are similar [147].

Increasing the deposition rate has so far not been successful as far as efficiency is concerned. Konagai et al. [55] obtained a rather low efficiency of 1.6% ($V_{oc} = 0.263$ V, $J_{sc} = 18.5$ mA/cm^2, FF = 0.323) for a poly Si cell (in the configuration glass/SnO_2/ZnO/p–i–n/ZnO/Ag/Al) where the i-layer was deposited at 1 nm/s. They attribute the low efficiency partly to contamination and partly to residual impurities from the chamber.

5.1.3. Grain boundaries

Using two-dimensional device modelling for a p–i–n based solar cell with a columnar grain structure, Takakura and Hamakawa [148] obtained a maximum

efficiency of 16% in a cell with optical confinement and a well passivated 10 μm microcrystalline Si i-layer with a grain size of 1 μm. The model included the grain boundary in the intrinsic layer oriented perpendicular to the cell junction. The carrier lifetime at the grain boundary was given by

$$1/\tau_{GB} = 1/\tau_{bulk} + S_{GB}/\Delta y,$$

where τ_{GB} is the lifetime at the grain boundaries, τ_{bulk} is the lifetime in the bulk, and Δy is the lattice point interval between a boundary position and its contiguous point in the side direction. The simulation showed that the highest recombination occurred at the p/i and i/n interfaces of the grain boundary. V_{oc} and FF were strongly affected by the grain size and the grain boundary defect density (mainly grain size below 0.5 μm), whereas J_{sc} was not affected by these parameters down to a grain size as low as 0.05 μm. This was attributed to an effective electron velocity larger than the recombination velocity at the grain boundary. Simulation also showed that acceptor doping in the intrinsic layer improved the efficiency, if the grain size was more than 0.3 μm. This was mostly due to the enhancement of V_{oc} and FF, although J_{sc} was reduced due to the doping. Werner [95] also reached a similar conclusion that a high open circuit voltage is achievable with (i) a large grain size and (ii) a small grain boundary recombination velocity. High efficiency poly/microcrystalline solar cells are possible at two extremes (i) very large grain size (in a high temperature process) for the p–n junction or (ii) very small grain size suitable for a p–i–n junction (in a low temperature process). The first case was simulated by a simple model, which employed a relationship between the effective diffusion length and the grain size and recombination velocity. Simulated curves (taking various recombination velocities) showed a good correlation with experimental observations, where a monotonic decrease of the open circuit voltage with grain size was found (Fig. 7). However, p–i–n microcrystalline solar cells show a high open circuit voltage even with a much smaller grain size. This is attributed to (i) the intrinsic nature of the layer, (ii) a low oxygen content, (iii) a high hydrogen content and (iv) selective growth of the grain boundaries with a small number of broken bonds. The intrinsic nature of the layer, together with the small grain size, reduces the band bending at the grain boundary, whereas a low oxygen content, high hydrogen content and special grain boundary reduce the grain boundary defect density. Together, they reduce the recombination velocity.

Using two-dimensional modelling for p–i–n type solar cells, where the intrinsic layer had a grain boundary in a flat surface perpendicular to the cell structure, Taretto et al. [149] predicted that the open circuit voltage would increase upon doping the i-layer. Their prediction fitted the open circuit voltage of the Kaneka Co. cells for a doping level of $\sim 10^{16}\,cm^{-3}$. This explains why Kaneka Co. uses a π-doped layer instead of intrinsic ones, as used by other groups such as IMT, Neuchatel. They also showed that p–n cells are much more sensitive to a defect rich surface than a p–π–n solar cells with a π-layer doping up to $3 \times 10^{17}/cm^3$.

The special grain boundary is a very interesting subject. An observation for most microcrystalline silicon p–i–n or n–i–p solar cells is that a high efficiency has been achieved with an i-layer having (2 2 0) oriented growth (Fig. 7). This lead to

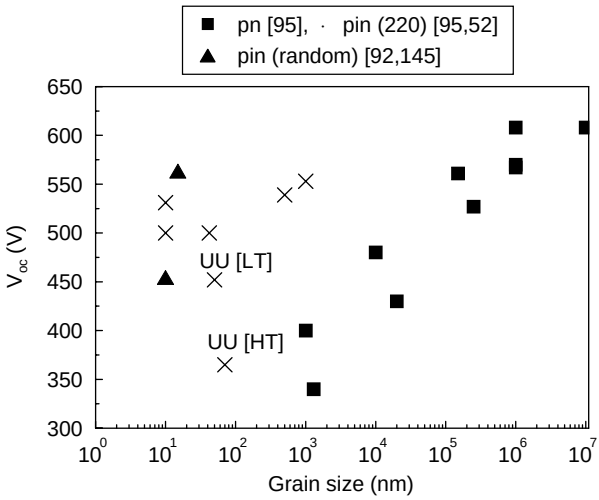

Fig. 7. Dependence of the open circuit voltage on the grain size, for various types of solar cell.

speculation that in such material, grain boundaries are [110] tilt type, which are known to be electrically inactive [150]. However, these boundaries can become electrically active if they contain impurities like oxygen. Kondo and Matsuda [151], in XRD spectra, observed a satellite line at a lower theta (26.6°) than the (1 1 1) line. This peak, with an intensity of 5% of the (1 1 1) line, is attributed to the Σ_3 twin grain boundary perpendicular to the substrate. Alhough these twin boundaries are electrically inactive, trapping at these sites is speculated to be responsible for the low open circuit voltage. Nozawa et al. [76] also observed this low angle side of the main (1 1 1) crystalline diffraction peak for a (2 2 0) preferentially oriented film grown by ECR CVD. This additional peak has been attributed to polytypic silicon modification. Fig. 8 shows the XRD spectra of a poly Si film made by HWCVD at Utrecht University. Both the samples are (2 2 0) oriented. However, sample a is an unoptimised one, in which peaks around (1 1 1) are observed. The satellite peak at $\sim 2\theta = 27^\circ$ in some cases (as shown here) has only slightly less intensity than the (1 1 1) peak. However, for the case of compact films we observe an exclusive (2 2 0) orientation. Sample b is a profiled layer, i.e., compact poly Si on a seed layer (the layer actually used in a solar cell) and it has no satellite line (also no (1 1 1) line). An interesting observation to be made from Fig. 7 is that there are reports of a high V_{oc} for solar cells with i-layers containing randomly oriented grains. Of course, other aspects such as grain size and the passivation of grain boundary defects also play equally important roles in achieving a high V_{oc}.

The advantage of a columnar structure for carrier collection in a solar cell is debatable. For example, in case of the HWCVD poly Si cells grown at Utrecht University [152], the crystalline orientation partly explains why the cells work so well, even though the defect density is still too high ($7.8 \times 10^{16}\,\mathrm{cm}^{-3}$) for carrier collection. Fig. 9 shows the sub-bandgap optical absorption spectrum of a poly Si:H

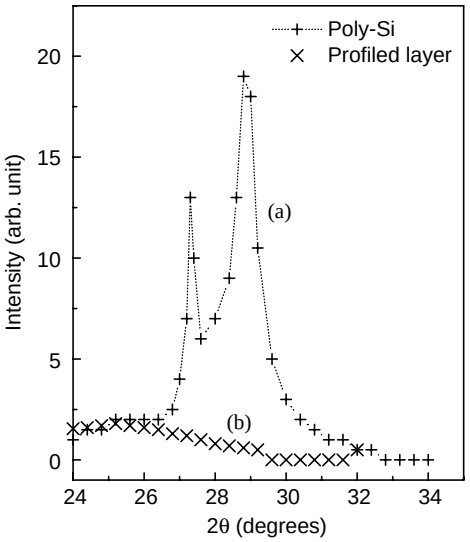

Fig. 8. X-ray diffraction data for two poly Si samples made by HWCVD at UU: (a) an unoptimised (2 2 0) oriented poly Si films, a satellite peak is at $\sim 2\theta = 27^{\circ}$, left to the (1 1 1) peak; (2) a profiled layer of Poly1/Poly2((2 2 0) oriented).

film. The spectrum measured by photothermal deflection spectroscopy (PDS) for a poly Si film on glass shows a considerable amount of absorption in the low-energy region, which is characteristic of the grain boundary defects. This is consistent with ESR results. However, the absorption spectrum measured by dual beam photoconductivity (DBP) of the same material incorporated in a cell configuration has characteristics similar to those of c-Si, i.e., the spectrum has an absorption edge at 1.1 eV. In the DBP measurement of the cell, the photoconductivity transport path is in the perpendicular direction. As the crystalline growth is columnar with a (2 2 0) preferential orientation of grains, the transport path in the cell is along the length of the columnar grains, thus bypassing the clustered defects between the columns. This model of the structure is indeed confirmed by cross-sectional TEM, where a columnar growth of the grains on the substrate is observed. The absence of any defect absorption in the DBP spectrum of the cell also indicates that there is no significant defect density within the grains. The diffusion length of the minority carriers (568 nm from SSPG) measured in the planar configuration is limited by the width of the columns, whereas in the cell configuration the carriers can diffuse along the length of the columns (extending over the thickness of the i-layer) without encountering defects.

Rezek et al. [153] studied local electronic transport (via a two-dimensional map of the dark conductivity) in microcrystalline silicon thin films (PECVD), by atomic force microscopy (AFM) with a conductive cantilever. Comparing the morphology with the current image, they found that a pronounced decrease in the currents at the grain boundaries was observed. They attributed this to the increased resistance of the

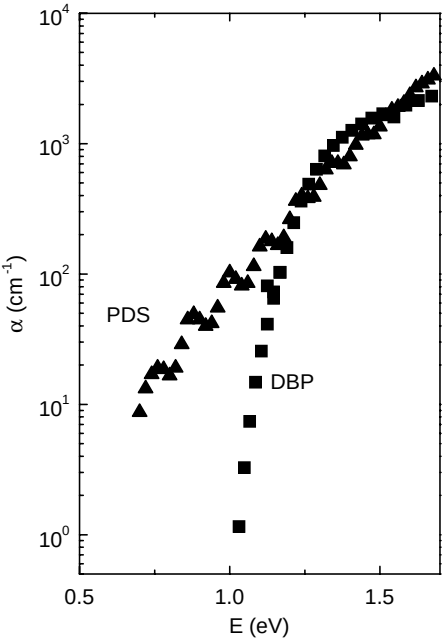

Fig. 9. Optical absorption coefficient of a HWCVD poly Si film made at Utrecht University [152]. The PDS spectrum was measured on an individual layer, and the DBP spectrum was measured for a film in a cell.

grain boundaries. This result indicates that a grain boundary cannot necessarily be treated as a high conductive path for shunting/leakage in a solar cell structure.

Rath et al. [116] studied an n–i–p poly Si cell using a one-dimensional AMPS (AMS1D) computer program. The device characteristics of n–i–p cells incorporating profiled poly Si:H films in the configuration SS/n-μc-Si:H(PECVD)/i-poly Si:H(HWCVD)/p-μc-Si:H(PECVD)/ITO was simulated using as an input parameter the defect distribution obtained from the SCLC, ESR and DBP techniques, and graded optical properties of the i-layer. The predictions were as follows. Transport of photogenerated carriers in the intrinsic layer of the cell is dominated by drift. However, a smaller but significant diffusion component (of the same order) to carrier transport is present. The drift component is relatively stronger for electron than for hole transport. A high defect density in the back region (at the n/i interface) of the poly Si reduces the efficiency of an n–i–p cell, because the field is weakened in the i-layer bulk, and recombination is enhanced in the back region. By proper passivation of defects in the seed layer or the use of a less defective seed layer, the efficiency can be further improved. The current–voltage (J–V) characteristics and the QE are insensitive to variations in the grain db densities within the range 10^{12}–$10^{15}\,\mathrm{cm}^{-3}$. The effect of the grain boundaries is essentially to control the field in the i-layer, whereas the photogenerated hole and electron transport are not hindered by it. This is in conformity with a model in which the photogenerated carriers bypass the grain

boundary defects (see Fig. 9), whereas in the dark (in thermal equilibrium) these defects take part in trapping (defects measured by SCLC), thus determining the field in the i-layer. The $J-V$ and QE under illumination are sensitive to the free carrier mobilities. The mobility values for the i-layer very near to the c-Si are necessary to simulate the experimental values of poly Si solar cells, though the Hall mobilities (in the coplanar configuration) are in the range 1–10 $cm^2/V s$. The efficiency is not sensitive to the n-layer thickness in the range 20–100 nm. This allows one to use a thick n-layer (50 nm) in the cell, to avoid shunting. The computer prediction showed that a maximum efficiency of 5.5% could be achieved for an i-layer thickness of 2.8 μm (without a back reflector or additional texturisation). The experimental spectral response could only be fitted (even using high mobilities) by using a graded optical gap for the i-layer, with the gap decreasing with increasing thickness of the poly Si.

In the next section, we will give the solar cell efficiencies for high temperature deposited poly Si films, to allow a comparison to those for the low temperature processes.

5.2. High temperature poly Si

Zone-melting recrystallisation (*ZMR*): By ZMR, Mitsubishi [154] has been able to obtain an efficiency of 16% on $10 \times 10\,cm^2$ area solar cells with polycrystalline silicon films of only 77 μm thickness using a VEST (etching of the underlying substrate through via-holes in the silicon film) process. VEST cells are made by first separating the active layer from the substrate and then fabricating the cell.

Liquid phase epitaxy: Cells on carbon substrates without a seed layer showed an efficiency of 10.2% on a 4.37 cm^2 area with a cell thickness of 30 μm [155]. Drift-field thin film solar cells with LPE layers on electrically inactive p^{++} CZ silicon substrates showed an efficiency of 16.4% [156]. The University of Constantz achieved an efficiency of 10% for a LPE poly Si cell. On a $ZrSiO_4$ substrate, the efficiency was 8.3%.

Lift-up from a porous substrate: Sony [157] achieved an efficiency of 12.5% for a 12 μm thick 4 cm^2 area solar cell obtained using a sacrificial porous silicon layer. By a layer transfer technique, an epitaxially grown silicon thin film layer on a silicon wafer (a quasi monocrystalline Si film in between the epitaxial Si film and the wafer) was transferred to glass before an emitter, front contact and SiN_x antireflection coating were made on this absorber layer [158]. By this process, an efficiency of 15.3% ($V_{oc} = 0.634$ V, FF = 0.803, $J_{sc} = 30.1\,mA/cm^2$) was achieved on a cell area of 1 cm^2 with an i-layer thickness of 23 μm. Modelling predicted an efficiency of 17–18% for a thickness of 25 μm on a glass substrate.

The SPC method: A thin film polycrystalline silicon cell on a metal substrate in the configuration metal/n^+ poly Si/poly Si/p-layer/ITO using 10 μm thick SPC poly Si i-layer [159] yielded an efficiency of 9.2% (FF = 0.664, $V_{oc} = 0.553$ V, $J_{sc} = 25\,mA/cm^2$).

It is clear that low temperature processed cells have comparatively lower efficiencies. At present, the effectiveness of low temperature poly Si cells can be

exploited only in tandem or multi-junction cells. In fact, it is the "micromorph" concept which brought enormous interest to this field. In the next section, we show some of the multijunction cell results, and modules and minimodules with their stabilised efficiencies.

5.3. Tandem cells

Tandem cells are made by combining a microcrystalline bottom cell with an amorphous silicon top cell to fully utilise the high efficiency of the a-Si cell in the short wavelength region of the solar spectrum. However, the stabilised efficiency of a tandem cell is important because of the degradation of the amorphous silicon top cell, although the μc-Si bottom cell is stable to light soaking.

Liao et al. [160] used a triode configuration in a 13.56 MHz frequency PECVD deposition to deposit a μc-Si i-layer for a solar cell made at a substrate temperature of 250°C. An enhanced deposition rate was achieved through an increase in power, and a deposition rate of 0.2 nm/s was obtained using a power density of 0.7 W/cm^2, for a SiH_4/H_2 ratio of 3%. Using this material for the bottom cell in a tandem configuration: Glass/SnO_2/buffer/p-a-SiC:H (10 nm)/grading (12 nm)/i-Si:H (200 nm)/n^+ μc-Si (10 nm)/buffer/p-μc-Si/i-μc-Si (1500 nm)/n^+μc-Si (30 nm)/Al, an efficiency of 8.91% ($V_{oc} = 1.16$ V, FF = 0.674, $J_{sc} = 11.4$ mA/cm^2) was obtained on a cell area of 0.126 cm^2.

For RF PECVD deposited superstrate type tandem solar cells (a-Si/μc-Si), Rech et al. [135] obtained an efficiency of 11.9% (FF = 0.717, $V_{oc} = 1.36$ V, $J_{sc} = 12.1$ mA/cm^2) on 30×30 cm^2 SnO_2 coated glass (Asahi) substrates, and an average efficiency of 11.0% was achieved. For a deposition rate of 0.6 nm/s with a 1.6 μm bottom cell [136], the efficiency was 11.1% (FF = 0.648, $V_{oc} = 1.34$ V, $J_{sc} = 11.7$ mA/cm^2).

For a stacked substrate type a-Si/poly Si/poly Si hybrid cell made by RF PECVD, Yamamoto et al. [30] obtained an efficiency of 12% after 550 h of degradation. The parameters were $V_{oc} = 1.84$ V, $J_{sc} = 8.54$ mA/cm^2 and FF = 0.762. A thinner amorphous layer in the triple cell configuration is the key to a low degradation. However, in a later development [134] in which a p–i–n type cell structure was used, it was shown that for stacked cells both p–i–n and n–i–p configurations showed similar performances, as the a-Si top cell contributed two thirds of the cell efficiency. In the superstrate structure [161], an initial efficiency of 14.1% ($J_{sc} = 13.6$ mA/cm^2, FF = 0.743, $V_{oc} = 1.392$ V) has been achieved for an a-Si:H/poly Si tandem cell of 1 cm^2 area. A transparent layer was used in between the top and bottom cells, which not only improved the optical generation of the top cell but also reduced the shunting problem. For a mini module (10×10 cm^2, 10 segments monolithically series connected) the efficiencies before and after degradation were 12.5% and 11.3%, respectively. They also achieved 11.7% ($I_{sc} = 0.452$, FF = 0.739, $V_{oc} = 134.3$ V) aperture area efficiency for an a-Si/poly Si integrated solar cell module of 91×45.5 cm^2 size. A stabilised efficiency of 10% has been achieved for such modules. It was shown that the real outdoor performance showed an output power of 46 W for a 43 W indoor-calibrated module. The temperature dependence of the

efficiency was similar to that of an a-Si cell rather than a poly Si cell, because two thirds of the power was generated by the a-Si top cell.

Meier et al. [4] achieved a 13.1% initial efficiency for a superstrate type a-Si/μc-Si tandem cell made by VHF-PECVD using the so-called "micromorph" concept. They achieved a stabilised efficiency of 10.7% (12% in natural sunlight, unconfirmed) for these cells [162]. A microporph (a-Si/poly Si) minimodule [163] of area 23.3 cm^2 having 6 segments showed an aperture area stable efficiency of 9.1% ($I_{sc} = 39.72$ mA, $V_{oc} = 8.014$ V, FF = 0.666). In-house LP-CVD ZnO deposited on glass was used as the substrate. A substrate type micromorph tandem cell (n–i–p/n–i–p) [140] showed an efficiency of 11.2% ($V_{oc} = 1.4$ V, FF = 0.71, $J_{sc} = 11.3$ mA/cm^2). For an n–i–p/n–i–p type stacked a-Si(0.4 μm)/μc-Si(1 μm) solar cell on a SS substrate, Saito et al. [141] showed a 13% initial and a 11.5% degraded cell efficiency for a μc-Si i-layer deposited at 0.2 nm/s, and a 12% initial efficiency for the one deposited at 0.5 nm/s, by VHF-CVD.

Using microcrystalline silicon grown by microwave PECVD for the bottom cells, Jones et al. [145] made tandem and triple junction cells with initial efficiencies of 9.8% and 11.4%, respectively [145]. These cells have been compared with the high quality a-SiGe:H cells typically used as the bottom cells for triple-junction a-Si/a-SiGe/a-SiGe solar cells, which were prepared at United Solar using a standard PECVD technique and an i-layer deposited at a rate of 0.1 nm/s. The lower J_{sc} values of the μc-Si cells infer that they do not absorb as much red light as a-SiGe cell. However, they absorb more light above 900 nm due to their low band gap. The P_{max} values of the μc-Si cells degrade by less than 5%, whereas those of a-SiGe cells degrade by 17%. The authors believe that μc-Si cells can best be used as replacements for the low band gap a-SiGe layers of triple junction cells, in which case the differences in the band gaps of μc-Si and a-SiGe are much less, and the demands for the longer wavelength response (800–1000 nm) are greater.

The best a-Si/poly Si tandem solar cell grown by HWCVD has been achieved by Rath et al. [164] on an n–i–p/n–i–p tandem configuration on a SS substrate. This had an efficiency of 8.08%. However, recent unpublished results reported an efficiency of 10.7% on a tandem cell [165].

5.4. Overview of solar cell efficiencies

The deposition rate and the process temperature are crucial parameters for the design of cell processing. In a roll-to-roll process, the deposition rate will define the length of the belt, whereas in a static process, the growth rate will determine the throughput. Both of these directly determine the cost of cell processing. Fig. 10 shows the relationship between the efficiencies and the growth rate for various deposition processes. The solar cell efficiencies show a definite correlation with deposition rate. Namely, the efficiencies monotonically decrease with increasing deposition rate. This can be attributed to general a deterioration of the microstructural quality at high growth rates, even while maintaining a high crystallinity. However, it is also observed that (for a few cases, recent developments) at low deposition rates, further improvements in the cell efficiencies are possible, and a record efficiency of

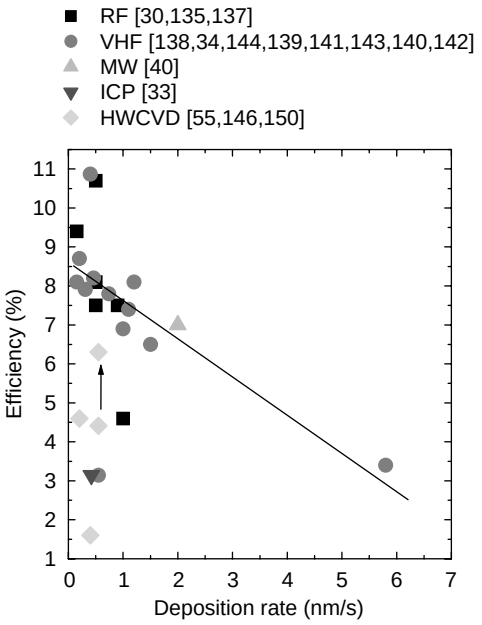

Fig. 10. Correlation of solar cell efficiencies of single-junction cells with the deposition rate, for samples grown by various deposition processes. The line is only a guide to the eye. The arrow shows the expected efficiency of a HWCVD cell (made at UU) if the back reflector is used.

10.87% has been achieved by Canon Co. at a deposition rate of 0.4 nm/s. However, as Canon Co. is developing this technique for roll-to-roll production, a further increase in the growth rate may be needed for a realistic belt design. Future research has to find a mechanism to improve the device performance at high deposition rates. Fig. 11 shows the dependence of the efficiency on substrate temperature. From this figure, two distinct regimes of growth are identified. (i) Low temperature (100–250°C): in these types of cell, materials are identified by small grains ($\sim$20 nm) and grain boundaries are passivated by a high hydrogen content. Cells from IMT Neuchatel [138], KFA Julich [140], and ETL [137] come under this category. (ii) High temperature (400–600°C): in these cells, materials are identified with large and $>$100 nm wide columnar grains, with the lengths of the grains being the same as the thickness of the film, compact structure and high (2 2 0) orientation. Examples are Kaneka Co. [30] and Utrecht University [52]. It is also observed that the low temperature grown cells are made at the transition between amorphous and crystalline silicon. No such regime has been identified in the high temperature processes. The distinction between the two processes is that the material has either a large grain boundary surface area but better passivation, or a reduced grain boundary region, but a lower hydrogen content to passivate. It must be mentioned that the exact deposition temperature of the Canon Co. cells [141] is not specified, which makes it difficult to put them in any category.

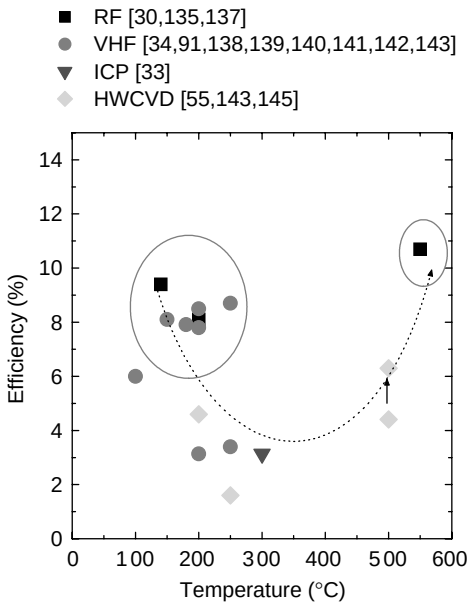

Fig. 11. Correlation of the solar cell efficiencies of single-junction cells with substrate temperature. The dotted line is only a guide to the eye. The dotted circles indicate the different temperature regimes to achieve high efficiency. The arrow indicates the expected efficiency of a HWCVD cell (made at UU) if a back reflector is used.

Reviewing all the solar cell results, it is apparent that a trend has been established to fabricate solar cells at a low crystalline volume fraction or at the transition between the microcrystalline and amorphous phases. This would pose a question as to how these cells behave when subjected to light soaking, considering the fact that a substantial amorphous component exists in the material. From the material studies, it is known that the degradation of μc-Si decreases with increase in grain size, and above grain size of 11.5 nm no degradation is observed [166]. This would clearly explain the virtually zero degradation of the poly Si cells made by the Kaneka Co. [167]. We have already mentioned that these cells made at high temperature contain large grained poly Si. The microcrystalline silicon cells of IMT [4] also show no degradation after exposure to a 10-sun intensity sodium light. Those cells had an initial efficiency of 7.7%. One may speculate that the grain size of $\sim$17 nm may be large enough, if this is considered to be the determining factor for degradation [166]. Due to the lack of degradation data for the recently developed high efficiency microcrystalline cells produced by various laboratories, no definite conclusions can be reached. The issue is still more important, especially for cells with high deposition rate microcrystalline materials made either by the HPD method or by microwave plasma. In this respect, the degradation results of Jones et al. [145] for the case of microwave plasma are interesting. The degradation of the cells is less for a higher crystalline volume fraction in the i-layer. It was observed that cells with a low

crystalline volume fraction degrade by 4.6%, whereas a high crystalline volume fraction leads to less than 1% degradation. More degradation data are required in future, if any definite statement is to be made on the stability aspects of microcrystalline cells.

6. Conclusions

An optimum substrate temperature, a high frequency for plasma deposition, and the reduction of ion impact are found to be the guiding parameters for achieving poly Si films at high deposition rates. However, this does not translate into the efficiency in solar cells. A correlation of decreasing efficiency with increasing deposition rate is observed, independent of the deposition method, although further improvement in efficiencies at low deposition rates has been observed in a few cases. Two distinct approaches in solar cell fabrication, namely, (i) small grained microcrystalline silicon (grown at temperatures below 300°C) and (ii) large grained poly Si grown in a high temperature (400–600°C) approach have been identified. Most reports (for the low temperature approach) claim their best efficiencies for films deposited in the transition region between amorphous and microcrystalline silicon growth. Various defect states in poly Si have been identified, and the DOS can be represented in a similar way to that of amorphous silicon, complete with midgap and tail states. An anisotropy in the electronic transport in these films has been identified and correlated with the device properties in solar cells. The true optical absorption has to be determined by excluding the scattering effect, in determining the band gap and defect density. A tremendous improvement in tandem and multijunction cell and module efficiencies has proved that this low temperature poly Si/microcrystalline silicon approach could lead to a boost to large area thin film silicon in industrial applications. The Kaneka Co., Japan, has already shown the way.

Appendix A. Abbreviations

1. Deposition

RF:	radio frequency
PECVD:	plasma enhanced chemical vapour deposition
VHF:	very high frequency
UHF:	ultra high frequency
ECR:	electron cyclotron resonance
HWCVD:	hot wire chemical vapour deposition
ETP:	expanding thermal plasma
ICP:	inductively coupled plasma
EBEP-CVD:	electron beam excited plasma chemical vapour deposition
TPCVD:	thermal plasma chemical vapour deposition
SCC-GD:	static closed chamber glow discharge

RLSA:	radial line slot antenna
SPC:	solid phase crystallisation
LP-CVD:	low pressure chemical vapour deposition
ZMR:	zone melting recrystallisation
LPE:	liquid phase epitaxy
IAPVD:	ion assisted physical vapour deposition
IASP:	ion assisted sputtering

2. Deposition parameters

HPD:	high-pressure depletion
T_s:	substrate temperature
T_{fill}:	filament temperature
Pr:	pressure

3. Materials

c-Si:	crystalline silicon
poly Si:	polycrystalline silicon
a-Si:	amorphous silicon
a-SiGe:	amorphous silicon germanium
μc-Si:	microcrystalline silicon
TCO:	transmitting conducting oxide
SS:	stainless steel
W:	tungsten
Ta:	tantalum
Ar:	argon
Ga:	galium
In:	indium
PES:	polyethersulfone
PET:	polyethylene terepthalate
Poly1:	poly silicon made at high hydrogen dilution (HWCVD at UU)
Poly2:	poly silicon made at low hydrogen dilution (HWCVD at UU)
ITO:	indium tin oxide
Cz:	Czocralski

4. Physical properties

V_{oc}:	open circuit voltage
FF:	fill factor
J_{sc}:	short circuit current density
η:	efficiency
I–V:	current voltage
QE:	quantum efficiency
CE:	conduction electron
db:	dangling bond
TD:	thermal donor
α:	absorption coefficient

$h\nu$:	energy
L:	diffusion length
σ:	conductivity
N_d:	defect density
Pa:	Pascal
V_f:	volume fraction
DOS:	density of states
RMS:	root mean square

5. Measurement

PDS:	photothermal deflection spectroscopy
CPM:	constant photocurrent method
DBP:	dual beam photoconductivity
XTEM:	cross-sectional transmission electron microscopy
ESR:	electron spin resonance
LESR:	light enhanced spin resonance
SDPC:	spin dependent photoconductivity
EDMR:	electrically detected magnetic resonance
SIMS:	secondary ion mass spectroscopy
IR:	infrared
TOF:	time of flight
SSPG:	steady-state photocarrier grating technique
SPV:	surface photovoltage
TRMC:	time resolved microwave conductivity
SE:	spectroscopic ellipsometry
AFM:	atomic force microscopy
SCLC:	space charge limited current

6. Laboratories

ETL:	Electro Technical Laboratory, Japan
UU:	Utrecht University
HMI:	Hahn Meitner Institute, Berlin
KFA:	Research Center Julich
IMT:	Institute of Microtechnology, Neuchatel

References

[1] L.L. Kazmerski, Tech. Digest Int. PVSEC-12, Jeju, Korea, 2001, p. 11.
[2] A. Goetzberger, J. Luther, G. Willeke, Tech. Digest Int. PVSEC-12, Jeju, Korea, 2001, p. 5.
[3] J. Meier, R. Fluckiger, H. Keppner, A. Shah, Appl. Phys. Lett. 65 (1994) 860.
[4] J. Meier, P. Torres, R. Platz, S. Dubail, U. Kroll, J.A.A. Selvan, N.P. Vaucher, Ch. Hof, D. Fischer, H. Keppner, A. Shah, K.-D. Ufert, P. Giannoules, J. Koehler, Mater. Res. Soc. Symp. Proc. 420 (1996) 3.
[5] E. Hamers, Ph.D.Thesis, Utrecht University, 1998.

[6] H. Keppner, U. Kroll, P. Torres, J. Meier, D. Fischer, M. Goetz, T. Tscharner, A. Shah, Proc. 25th IEEE Photovoltaic Specialist Conference, 1996, p. 669.
[7] M. Kondo, A. Matsuda, Thin Solid Films 383 (2001) 1.
[8] S. Veprek, F.-A. Sarrott, Z. Iqbal, Phys. Rev. 36 (1987) 3344.
[9] A. Matsuda, J. Non. Cryst. Solids 59/60 (1983) 767.
[10] H. Shirai, K. Yoshino, G. Ogawara, H. Ueyama, Tech. Digest Int. PVSEC-12, Jeju, Korea, 2001, p. 795.
[11] T. Nishimiya, M. Kondo, A. Matsuda, Mater. Res. Soc. Symp. Proc. 467 (1997) 397.
[12] W. Shindoh, T. Ohmi, J. Appl. Phys. 79 (1996) 2347.
[13] A. Matsuda, K. Kumagai, K. Tanaka, Jpn. J. Appl. Phys. 22 (1983) L34.
[14] W.J. Varhue, J.L. Rogers, P.S. Andry, E. Adams, Appl. Phys. Lett. 68 (1996) 349.
[15] S. DeBoer, V.L. Dalal, R. Bartel, G. Chumanov, Appl. Phys. Lett. 66 (1995) 2528.
[16] R. Nozawa, H. Takeda, M. Ito, M. Hori, T. Goto, J. Appl. Phys. 81 (1997) 8035.
[17] M. Birkholz, B. Selle, W. Fuhs, D. Williamson, Mater. Res. Soc. Symp. Proc. 664 (2001) A15.4.1.
[18] R. Nozawa, K. Murata, M. Ito, M. Hori, T. Goto, J. Vac. Sci. Technol. A 17 (1999) 2542.
[19] S. Bae, A.K. Kalkan, S. Cheng, S.J. Fonash, J. Vac. Sci. Technol. A 16 (1998) 1912.
[20] J. Joo, J. Vac. Sci. Technol. A 18 (4) (2000) 2006.
[21] J.H. Shin, H. Huh, J. Vac. Sci. Technol. A 18 (2000) 51.
[22] T.A. Wagner, L. Oberbeck, M. Nerding, H.P. Strunk, R.B. Bergmann, Mater. Res. Soc. Symp. Proc. 664 (2001) A22.3.1.
[23] M. Imaizumi, K. Okitsu, M. Yamaguchi, T. Ito, I. Konomi, M. Tokai, K. Kawamura, J. Vac. Sci. Technol. A 16 (5) (1998) 3134.
[24] E.A.G. Hamers, A.H.M. Smets, C. Smit, J.P.M. Hoefnagels, W.M.M. Kessels, M.C.M. van der Sanden, Mater. Res. Soc. Symp. Proc. 664 (2001) A421.
[25] E.A.G. Hamers, A. Fontcuberta i Morral, C. Niikura, R. Brenot, P. Roca i Cabarrocas, J. Appl. Phys. 89 (2000) 3674.
[26] M. Kondo, S. Yamasaki, A. Matsuda, J. Non-Cryst. Solids 266–269 (2000) 544.
[27] M.R. Wertheimer, M. Moisan, J. Vac. Sci. Technol. A 3 (1985) 2643.
[28] J. Dutta, U. Kroll, P. Chabloz, A. Shah, A.A. Howling, J.-L. Dorier, Ch. Hollenstein, J. Appl. Phys. 72 (1992) 3220.
[29] L. Guo, M. Kondo, M. Fukawa, K. Saitoh, A. Matsuda, Jpn. J. Appl. Phys. 37 (1998) L1116.
[30] K. Yamamoto, M. Yoshimi, Y. Tawada, Y. Okamoto, A. Nakajima, J. Non-Cryst. Solids 266–269 (2000) 1082.
[31] A.H. Jayatissa, Y. Htanaka, Y. Nakanishi, T. Yamaguchi, Jpn. J. Appl. Phys. 35 (1996) 5687.
[32] S. Koynov, R. Schwarz, T. Fischer, S. Grebner, H. Munder, Jpn. J. Appl. Phys. 33 (1994) 4534.
[33] B.Y. Moon, J.H. Youn, S.H. Won, J. Jang, Sol. Energy Mater. Sol. Cells 69 (2001) 139.
[34] S. Suzuki, M. Kondo, A. Matsuda, Tech. Digest Int'l PVSEC-12, Korea, 2001, p. 559.
[35] L. Feitknecht, J. Meier, P. Torres, J. Zurcher, A. Shah, Tech. Digest Int. PVSEC-12, Jeju, Korea, 2001, p. 459.
[36] S. Takashima, M. Hori, T. Goto, K. Yoneda, J. Appl. Phys. 89 (2001) 4727.
[37] B. Moradi, V.L. Dalal, R. Knox, J. Vac. Sci. Technol. A 12 (1994) 251.
[38] B.B. Jagannathan, R.L. Wallace, W.A. Anderson, J. Vac. Sci. Technol. A 16 (1998) 2751.
[39] K. Nakahata, A. Miida, T. Kamiya, C.M. Fortmann, I. Shimizu, Thin Solid Films 337 (1999) 45.
[40] S.J. Jones, R. Crucet, X. Deng, D.L. Williamson, M. Izu, Mater. Res. Soc. Symp. Proc. 609 (2000) A15.1.1.
[41] W. Soppe, C. Deville, H. Donker, J.K. Rath, Mater. Res. Soc. Symp. Proc. (2002).
[42] Y. Sakuma, L. Haiping, H. Ueyama, H. Shirai, Vacuum 59 (2000) 266.
[43] H. Shirai, K. Yoshino, G. Ohkawara, H. Ueyama, Jpn. J. Appl. Phys. 40 (2001) L701.
[44] W. Shindo, S. Sakai, H. Tanaka, C.J. Zhong, T. Ohmi, J. Vac. Sci. Technol. A. 17 (1999) 3134.
[45] J.H. Jang, K.S. Lim, Jpn. J. Appl. Phys. (Part I) 35 (1996) 5625.
[46] H. Matsumura, Jpn. J. Appl. Phys. 30 (1991) L1522.
[47] H. Matsumura, Y. Tashiro, K. Sasaki, S. Furukawa, Jpn. J. Appl. Phys. 33 (1994) L1209.
[48] J. Cifre, J. Bertomeu, J. Puigdollers, M.C. Polo, J. Andreu, A. Lloret, Appl. Phys. A 59 (1994) 645.

[49] J. Puigdollers, J. Bertomeu, J. Cifre, J. Andreu, J.C. Delgado, Mater. Res. Soc. Symp. Proc. 377 (1995) 63.
[50] A.R. Middya, J. Guillet, J. Perrin, A. Lloret, J.E. Bouree, Proceedings of the 13th European Photovoltaic Conference and Exhibition, Nice, 1996, p. 1704.
[51] J.K. Rath, H. Meiling, R.E.I. Schropp, Jpn. J. Appl. Phys. 36 (1997) 5436.
[52] J.K. Rath, F.D. Tichelaar, R.E.I. Schropp, Solid State Phenom. 67–68 (1999) 465;
R.E.I. Schropp, J.K. Rath, IEEE Trans. Electron. Devices 46 (10) (1999) 2069.
[53] M. Komoda, K. Kamesaki, A. Masuda, H. Matsumura, Thin Solid Films 395 (2001) 198.
[54] H. Matsumura, Thin Solid Films 395 (2001) 1.
[55] M. Konagai, T. Tsushima, M. Kim, K. Asakusa, A. Yamada, Y. Kudriavtsev, A. Villegas, R. Asomoza, Thin Solid Films 395 (2001) 152;
M. Konagai, T. Tsushima, Y. Ide, K. Asakusa, T. Fujisaki, M.K. Kim, Y. Wakita, A. Yamada, Conference Record of the 28th IEEE Photovoltaic Specialists Conference-2000, Anchorage, 2000, p. 788.
[56] T. Watahiki, K. Abe, H. Tamura, S. Miyajima, A. Yamada, M. Konagai, Thin Solid Films 395 (2001) 221.
[57] K. Bruhne, M.B. Schubert, C. Kohler, J.H. Werner, Thin Solid Films 395 (2001) 163.
[58] J.C. Lee, K.H. Kang, S.K. Kim, K.H. Yoon, J. Song, I.J. Park, Thin Solid Films 395 (2001) 188.
[59] Y. Feng, M. Zhu, F. Liu, J. Liu, H. Han, Y. Han, Thin Solid Films 395 (2001) 213.
[60] T. Ito, H. Inouchi, K. Ohkado, K. Chikusa, N. Nakamura, H. Kondo, N. Yoshida, S. Nonomura, Thin Solid Films 395 (2001) 217.
[61] J. Meier, H. Keppner, S. Dubail, Y. Ziegler, L. Feitnecht, P. Torres, Ch. Hof, U. Kroll, D. Fischer, J. Cuperus, J.A. Anna Selvan, A. Shah, Second World Conference and Exhibition on Photovoltaic Solar Energy Conversion, Viena, 1998, p. 375.
[62] V.L. Dalal, Thin Solid Films 395 (2001) 173.
[63] A. Masuda, K. Kamesaki, A. Izumi, H. Matsumura, Mater. Res. Soc. Symp. Proc. 664 (2001) A4.5.1.
[64] D. Franz, F. Grangeon, T. Delachaux, A.A. Howling, Ch. Hollenstein, J. Karner, Thin Solid Films 383 (2001) 11.
[65] R. Reinig, F. Fenske, B. Selle, W. Fuhs, Mater. Res. Soc. Symp. Proc. 664 (2001) A5.7.1.
[66] Y. Chae, H. Ohno, K. Eguchi, T. Yoshida, Mater. Res. Soc. Symp. Proc. 664 (2001) A4.4.1.
[67] T.H. Wang, T.F. Ciszek, M. Page, Y. Yan, R. Bauer, Q. Wang, J. Casey, R. Reedy, R. Matson, R. Ahrenkiel, M.M. Al-Jassim, Conference Record of the 28th IEEE Photovoltaic Specialists Conference-2000, Anchorage, 2000, p. 138.
[68] T. Arai, H. Shirai, J. Appl. Phys. 80 (1996) 4976.
[69] J. Zhou, K. Ikuta, T. Yasuda, T. Umeda, S. Yamasaki, K. Tanaka, Appl. Phys. Lett. 71 (1997) 1534.
[70] A. Heya, A. Izumi, A. Masuda, H. Matsumura, Jpn. J. Appl. Phys. (I) 39 (2000) 3888.
[71] S. Ishihara, D. He, M. Nakata, I. Shimizu, Jpn. J. Appl. Phys. 32 (1993) 1539.
[72] S. Ishihara, D. He, I. Shimizu, Jpn. J. Appl. Phys. 33 (1994) 51.
[73] J.K. Rath, F.D. Tichelaar, H. Meiling, R.E.I. Schropp, Mater. Res. Soc. Symp. Proc. 507 (1998) 879.
[74] C. Wang, M.J. Willams, G. Lucovsky, J. Vac. Sci. Technol. A 9 (1991) 444.
[75] J.E. Bouree, Thin Solid Films 395 (2001) 157.
[76] R. Nozawa, H. Takeda, M. Ito, M. Hori, T. Goto, J. Appl. Phys. 81 (1997) 8035.
[77] P. Roca i Cabarrocas, N. Layadi, M. Kunst, C. Clerc, H. Bernas, J. Vac. Sci. Technol. A 16 (2) (1998) 436.
[78] H. Liu, S. Jung, Y. Fujimura, Y. Toyoshima, H. Shirai, Jpn. J. Appl. Phys. 40 (2001) L215.
[79] G. Cicala, P. Capezzuto, G. Bruno, J. Vac. Sci. Technol. A 19 (2001) 515.
[80] S. Bae, S.J. Fonash, J. Vac. Sci. Technol. A 17 (1999) 1987.
[81] P. Alpuim, V. Chu, J.P. Conde, J. Appl. Phys. 86 (1999) 3812.
[82] F. Finger, J. Muller, C. Malten, R. Carius, H. Wagner, J. Non. Cryst. Solids 266–269 (2000) 511.
[83] M. Vanecek, A. Poruba, Z. Remes, J. Rosa, S. Kamba, V. Vorlicek, J. Meier, A. Shah, J. Non-Cryst. Solids 266–269 (2000) 519.

[84] J.K. Rath, A. Barbon, R.E.I. Schropp, J. Non-Cryst. Solids 266–269 (1999) 548.
[85] N.H. Nickel, E.A. Schiff, Phys. Rev. B 58 (1998) 1114.
[86] T. Ehara, T. Ikoma, K. Akiyama, S. Tero-Kubota, J. Appl. Phys. 88 (2000) 1698.
[87] D. Will, C. Lerner, W. Fuhs, K. Lips, Mater. Res. Soc. Symp. Proc. 467 (1997) 361.
[88] M. Stutzmann, M.S. Brandt, M.W. Bayer, J. Non-Cryst. Solids 266–269 (2000) 1.
[89] P. Kanschat, K. Lips, W. Fuhs, J. Non-Cryst. Solids 266–269 (2000) 524.
[90] J.H. Werner, in: J.H. Werner, H.J. Moller, H.W. Strunck (Eds.), Springer Proceedings in Physics, Vol. 35, Springer, Berlin, 1989, pp. 345.
[91] M. Luysberg, C. Scholten, L. Houben, R. Carius, F. Finger, O. Vetterl, Mater. Res. Soc. Symp. Proc. 664 (2001) A15.2.1.
[92] O. Vetterl, F. Finger, R. Carius, P. Hapke, L. Houben, O. Kluth, A. Lambertz, A. Muck, B. Rech, H. Wagner, Sol. Energy Mater. Sol. Cells 62 (2000) 97.
[93] E. Vallat-Sauvain, U. Kroll, J. Meier, A. Shah, J. Appl. Phys. 87 (2000) 3137.
[94] J. Meier, E. Vallat-Sauvain, S. Dubail, U. Kroll, J. Dubail, S. Golay, L. Feitknecht, P. Torres, S. Fay, D. Fischer, A. Shah, Sol. Energy Mater. Sol. Cells 66 (2001) 73.
[95] J. Werner, in: M. Konagai (Ed.), Tech. Digest 13th Sunshine Workshop on Thin Film Solar Cells, NEDO, Tokyo, 2000, p. 41.
[96] T. Kitagawa, M. Kondo, A. Matsuda, J. Non-Cryst. Solids 266–269 (2000) 64.
[97] C.H. Seager, D.J. Sharp, J.K.G. Panitz, J. Vac. Sci. Technol. 20 (3) (1982) 430.
[98] L.L. Kazmerski, J.R. Dick, J. Vac. Sci. Technol. A 2 (2) (1984) 1120.
[99] L.L. Kazmerski, A.J. Nelson, R.G. Dhere, A. Yahia, F. Abou-Elfotouh, J. Vac. Sci. Technol. A 6 (3) (1988) 100.
[100] F. Liu, M. Zhu, Y. Feng, Y. Han, J. Liu, Thin Solid Films 395 (2001) 97.
[101] P. Torres, J. Meier, R. Fluckiger, U. Kroll, J.A. Anna-Selvan, H. Keppner, A. Shah, S.D. Littlewood, I.E. Kelly, P. Giannoules, Appl. Phys. Lett. 69 (1996) 1373.
[102] J. Meier, R. Fluckiger, H. Keppner, A. Shah, Appl. Phys. Lett. 65 (1994) 860.
[103] U. Kroll, J. Meier, H. Keppner, S.D. Littlewood, I.E. Kelly, P. Giannoules, A. Shah, Mater. Res. Soc. Symp. Proc. 337 (1995) 39.
[104] T. Kamei, T. Wada, A. Matsuda, Mater. Res. Soc. Symp. Proc. 664 (2001) A10.1.1.
[105] O. Vetterl, F. Finger, R. Carius, P. Hapke, L. Houben, O. Kluth, A. Lambertz, A. Muck, B. Rech, H. Wagner, Sol. Energy Mater. Sol. Cells 62 (2000) 97.
[106] Y. Saito, M. Aomori, H. Kuwano, J. Appl. Phys. 81 (2) (1997) 754.
[107] Y. Nasuno, M. Kondo, A. Matsuda, Appl. Phys. Lett. 78 (2001) 2330.
[108] R. Platz, S. Wagner, Appl. Phys. Lett. 73 (1998) 1236;
R. Platz, S. Wagner, J. Vac. Sci. Technol. A 16 (1998) 3218.
[109] H. Matsumura, Thin Solid Films 395 (2001) 1.
[110] M. Schubert, R. Bruggemann, G. Bilger, A. Hierzenberger, Proceedings of the Second World Conference and Exhibition on Photovoltaic Solar Energy Conversion, Viena, 1998, p. 834.
[111] R.E.I. Schropp, P.F.A. Alkemade, J.K. Rath, Sol. Energy Mater. Sol. Cells 65 (1–4) (2001) 541–547.
[112] Yoo Yeong Cho, K.S. Lim, Jpn. J. Appl. Phys. 36 (1997) 1094.
[113] F. Diehl, B. Schroder, H. Oechsner, J. Appl. Phys. 84 (1998) 3416;
F. Diehl, M. Scheib, B. Schroder, H. Oechsner, J. Non-Cryst. Solids 227–230 (1998) 973.
[114] A. Poruba, A. Fejfar, Z. Remes, J. Springer, M. Vanecek, J. Kocka, J. Meier, P. Torres, A. Shah, J. Appl. Phys. 88 (2000) 148;
M. Vanecek, A. Poruba, Z. Remes, N. Beck, M. Nesladek, J. Non-Cryst Solids 227–230 (1998) 967.
[115] P.A.T.T. van Veenendaal, J.K. Rath, R.E.I. Schropp, Proceedings of the 16th European Photovoltaic Solar Energy Conference, Glasgow, May 2000, p. 458.
[116] J.K. Rath, F.A. Rubinelli, M. van Veghel, C.H.M. van der Werf, Z. Hartman, R.E.I. Schropp, Proceedings of the 16th European Photovoltaic Conference and Exhibition, Glasgow, 2000, p. 462.
[117] A. Fejfar, N. Beck, H. Stuchlikova, N. Wyrsch, P. Torres, J. Meier, A. Shah, J. Kocka, J. Non-Cryst. Solids 227–230 (1998) 1006.
[118] J. Kudrna, F. Trojanek, P. Maly, I. Pelant, Appl. Phys. Lett. 79 (2001) 626.

[119] J. Kocka, A. Fejfar, P. Fojtik, K. Luterova, I. Pelant, B. Rezek, H. Stuchlikova, J. Stuchlik, V. Svrcek, Sol. Energy Mater. Sol. Cells 66 (2001) 61.
[120] V. Svrcek, I. Pelant, J. Kocka, P. Fojtik, B. Rezek, H. Stuchlikova, A. Fejfar, J. Stuchlik, A. Poruba, J. Tousek, J. Appl. Phys. 89 (2001) 1800.
[121] J. Kocka, J. Stuchlik, H. Stuchlikova, V. Svrcek, P. Fojtik, T. Mates, K. Luterova, A. Fejfar, Appl. Phys. Lett. 79 (2001) 2540.
[122] K. Nakahata, T. Kamiya, C.M. Fortmann, I. Shimizu, H. Stuchlikova, A. Fiefar, J. Kocka, J. Non-Cryst. Solids 266–269 (2000) 341.
[123] P.U. Jepsen, W. Schairer, I.H. Libon, U. Lemmer, N.E. Hecker, M. Birkholz, K. Lips, M. Schall, Appl. Phys. Lett. 79 (2001) 1291.
[124] R. Brenot, R. Vanderhaghen, B. Drevillon, P. Roca i Cabaroccas, Appl. Phys. Lett. 74 (1999) 58.
[125] R. Brenot, et al., J. Non-Cryst. Solids 266–269 (2000) 336.
[126] P.A.T.T. van Veenendaal, T.J. Savenije, J.K. Rath, R.E.I. Schropp, Thin Solid Films 403–404 (2002) 175.
[127] J. Meier, S. Dubail, S. Golay, U. Kroll, S. Fay, E.V. Vallat-Sauvain, L. Feitknecht, J. Dubail, A. Shah, Tech. Digest Int. PVSEC-12, Jeju, Korea, 2001, p. 783.
[128] M. Luysberg, C. Scholten, L. Houben, R. Carius, F. Finger, O. Vetterl, Mater. Res. Soc. Symp. Proc. 664 (2001) A15.2.1.
[129] Y. Nasuno, M. Kondo, A. Matsuda, Mater. Res. Symp. Proc. 664 (2001) A15.5.1;
Y. Nasuno, M. Kondo, A. Matsuda, Tech. Digest Int. PVSEC-12, Jeju, 2001, p. 791.
[130] E. Vallat-Sauvain, S. Fay, S. Dubail, J. Meier, J. Bailat, U. Kroll, A. Shah, Mater. Res. Soc. Symp. Proc. 664 (2001) A15.3.1.
[131] B. Ahn, D. Kim, J. Yoo, J. Yi, Conference Record of the 28th IEEE Photovoltaic Specialists Conference, Anchorage, 2000, p. 841.
[132] T. Yamamoto, M. Kondo, A. Matsuda, Tech. Digest Int. PVSEC-12, Jeju, Korea, 2001, p. 471.
[133] J.K. Rath, R.E.I. Schropp, Sol. Energy Mater. Sol. Cells 53 (1998) 189.
[134] K. Yamamoto, M. Yoshimi, T. Suzuki, T. Nakata, T. Sawada, A. Nakajima, K. Hayashi, Conference Record of the 28th IEEE Photovoltaic Specialists Conference-2000, Anchorage, 2000, p. 1428.
[135] B. Rech, O. Kluth, T. Repmann, T. Roschek, J. Springer, J. Muller, F. Finger, H. Stiebig, H. Wagner, Tech. Digest Int. PVSEC-12, Jeju, Korea, 2001, p. 339;
T. Roschek, T. Repmann, J. Muller, B. Rech, H. Wagner, Conference Record of the 28th IEEE Photovoltaic Specialists Conference, Anchorage, 2000, p. 150.
[136] B. Rech, T. Roschek, J. Muller, S. Wieder, H. Wagner, Sol. Energy Mater. Sol. Cells 66 (2001) 267;
T. Roschek, B. Rech, W. Beyer, P. Werner, F. Edelman, A. Chack, R. Weil, R. Beserman, Mater. Res. Soc. Symp. Proc. 664 (2001) A25.5.1.
[137] Y. Nasuno, M. Kondo, A. Matsuda, Jpn. J. Appl. Phys. 40 (2001) L303.
[138] J. Meier, Sol. Energy Mater. Solar Cells 66 (2001) 73.
[139] L. Feitnecht, O. Kluth, Y. Ziegler, X. Niquille, P. Torres, J. Meier, N. Wyrsch, A. Shah, Sol. Energy Mater. Sol. Cells 66 (2001) 397.
[140] O. Vetterl, A. Dasgupta, A. Lambertz, H. Stiebig, F. Finger, H. Wagner, Mater. Res. Symp. Proc. 664 (2001) A25.8.1.
[141] K. Saito, M. Sano, A. Sakai, R. Hayasi, K. Ogawa, Tech. Digest Int. PVSEC-12, Jeju, Korea, 2001, p. 429.
[142] K. Saito, M. Sano, K. Matuda, T. Kondo, T. Nishimoto, K. Ogawa, I. Kajita, Second World Conference and Exhibition on Photovoltaic Solar Energy Conversion, Viena, 1998, p. 351.
[143] T. Matsui, M. Tsukiji, H. Saika, T. Toyama, H. Okomoto, Tech. Digest Int'l. PVSEC-12, Jeju, Korea, 2001, p. 355.
[144] H. Mase, M. Kondo, A. Matsuda, Extended Abstract Int'l PVSEC-12, Korea, 2001, p. 473.
[145] S.J. Jones, R. Crucet, R. Capangpangan, M. Izu, A. Banerjee, Mater. Res. Soc. Symp. Proc. 664 (2001) A4.5.1;
S.R. Jones, R. Crucet, M. Izu, Conference Record of the 28th IEEE Photovoltaic Specialists Conference, Anchorage, 2000, p. 134.

[146] C. Niikura, S.Y. Kim, B. Drevillion, Y. Poissant, P. Roca i Cabarrocas, J.E. Bouree, Thin Solid Films 395 (2001) 178.
[147] O. Vetterl, A. Gross, A. Dasgupta, A. Lambertz, F. Finger, H. Wagner, Presented at 17th EPVSECE, Munich, 2001.
[148] H. Takakura, Y. Hamakawa, Tech. Digest Int'l PVSEC-12, Korea, 2001, p. 347.
[149] K. Taretto, U. Rau, J.H. Werner, Solid State Phenom. 80–81 (2000) 311.
[150] J.K. Rath, R.E.I. Schropp, W. Beyer, Solid State Phenom. 80–81 (2001) 109.
[151] M. Kondo, A. Matsuda, Thin Solid Films 383 (2001) 1.
[152] J.K. Rath, A. Barbon, R.E.I. Schropp, J. Non-Cryst. Solids 227–230 (1998) 1277.
[153] B. Rezek, J. Stuchlik, A. Fejfar, J. Kocka, Appl. Phys. Lett. 75 (1999) 1475.
[154] S. Ito, Y. Kitagawa, T. Mishima, T. Yokoyama, in: Saito, T. (Ed.), Technical Digest of the 11th International Photovoltaic Science and Engineering Conference, Hakkaido, Japan, 1999, p. 539.
[155] G.F. Zheng, W. Zhang, Z. Shi, D. Thorp, M.A. Green, 25th IEEE Photovoltaic Specialist Conference, Washington, 1996, p. 693.
[156] H. Tayanaka, K. Yamauchi, T. Matsushita, in: Saito, T. (Ed.), Technical Digest of the 11th International Photovoltaic Science and Engineering Conference, Hakkaido, Japan, 1999, p. 543.
[157] R.B. Bergmann, T.J. Rinke, C. Berge, J. Schmidt, J.H. Werner, Technical Digest of the 12th International Photovoltaic Science and Engineering Conference, Jeju, Korea, 2001, p. 29.
[158] T. Baba, M. Shima, T. Matsuyama, S. Tsuge, K. Wakisaka, S. Tsuda, Proceedings of the 13th EPVSEC, Nice, 1995, p. 1708.
[159] X. Liao, S. Sheng, F. Yun, Z. Ma, G. Kong, Y. Zhao, S. He, Z. Li, Sol. Energy Mater. Sol. Cells 49 (1997) 171.
[160] K. Yamammoto, M. Yoshimi, Y. Tawada, S. Fukuda, T. Sawada, T. Meguro, H. Takata, T. Suezaki, Y. Koi, K. Hayashi, T. Suzuki, A. Nakajima, Tech. Digest Int. PVSEC-12, Jeju, Korea, 2001, p. 547.
[161] J. Meier, S. Dubail, J. Cuperus, U. Kroll, R. Platz, P. Torres, J.A.A. Selvan, P. Pernet, N. Beck, N.P. Vaucher, Ch. Hof, D. Fischer, H. Keppner, A. Shah, J. Non-Cryst. Solids 227–230 (1998) 1250.
[162] S. Golay, J. Meier, S. Dubail, S. Fay, U. Kroll, A. Shah, Conference Record of the 28th IEEE Photovoltaic Specialists Conference, Anchorage, 2000, p. 1456.
[163] H. Morikawa, Y. Kwama, Y. Matsuno, S. Hamamoto, K. Imada, T. Ishihara, K. Kojima, T. Ogama, in: T. Saito (Ed.), Technical Digest of the 11th International Photovoltaic Science and Engineering Conference, Hakkaido, Japan, 1999, p. 529.
[164] J.K. Rath, B. Stannowski, P.A.T.T. van Veenendaal, M.K. van Veen, R.E.I. Schropp, Thin Solid Films 395 (2001) 320.
[165] S. Klein, F. Finger, R. Carius, O. Kluth, L.B. Neto, H. Wagner, M. Stutzmann, Presented at the 17th EPVSECE, Munich, 2001.
[166] H. Liu, M. Xu, Solid State Commun. 58 (1986) 601.
[167] K. Yamamoto, M. Yoshimi, Y. Tawada, Y. Okamoto, A. Nakajima, S. Igari, Appl. Phys. A 69 (1999) 179.